U.S. Department of Transportation

Federal Railroad Administration

Ballast Fouling Measurement Tool: Phase 1

Office of Research,
Development
and Technology
Washington, DC 20590

DOT/FRA/ORD-18/33

Final Report
September 2018

REPORT DOCUMENTATION PAGE

Form Approved
OMB No. 0704-0188

1. AGENCY USE ONLY (Leave blank)	2. REPORT DATE	3. REPORT TYPE AND DATES COVERED
	September 2018	Technical Report 12/2014

4. TITLE AND SUBTITLE
Ballast Fouling Measurement Tool: Phase 1

5. FUNDING NUMBERS
DTFR53-13-C-00061

6. AUTHOR(S)
Charles P. Oden, Carlton L. Ho, Hamed F. Kashani, Stanley S. Smith

7. PERFORMING ORGANIZATION NAME(S) AND ADDRESS(ES)
Earth Science Systems, LLC
11485 W. I-70 Frontage Rd., Unit B
Wheat Ridge, CO 80033

8. PERFORMING ORGANIZATION REPORT NUMBER

9. SPONSORING/MONITORING AGENCY NAME(S) AND ADDRESS(ES)
U.S. Department of Transportation
Federal Railroad Administration
Office of Railroad Policy and Development
Office of Research, Development and Technology
Washington, DC 20590

10. SPONSORING/MONITORING AGENCY REPORT NUMBER
DOT/FRA/ORD-18/33

11. SUPPLEMENTARY NOTES
COR: Hugh Thompson

12a. DISTRIBUTION/AVAILABILITY STATEMENT
This document is available to the public through the FRA Web site at http://www.fra.dot.gov.

12b. DISTRIBUTION CODE

13. ABSTRACT (Maximum 200 words)
A prototype man-portable ballast inspection instrument was developed by Earth Science Systems, LLC (ESS) at their facility for use by track inspectors based on ground penetrating radar (GPR) called the RAdar Ballast Inspection Tool (RABIT). During this study, it was determined that the RABIT system worked well for assessing the moisture of ballast. A collection of software routines was created for modeling and analyzing GPR data. One routine worked well when measurements were made at a single location, and another when continuous measurements were made along the track. A series of full-scale ballast models were created with a range of ballast conditions. GPR measurements from these models provided a reference dataset for calibrating the analysis routines. The system was preliminarily tested at the Union Pacific Railroad (UP) Rocky Siding track site. Finally, recommendations were made for building a small handheld system for easy spot measurements, and another system mounted to a small track dolly for more detailed measurements.

14. SUBJECT TERMS
Ground penetrating radar, GPR, RAdar Ballast Inspection Tool, RABIT, ballast, fouling, moisture

15. NUMBER OF PAGES
51

16. PRICE CODE

17. SECURITY CLASSIFICATION OF REPORT	18. SECURITY CLASSIFICATION OF THIS PAGE	19. SECURITY CLASSIFICATION OF ABSTRACT	20. LIMITATION OF ABSTRACT
Unclassified	Unclassified	Unclassified	

METRIC/ENGLISH CONVERSION FACTORS

ENGLISH TO METRIC

LENGTH (APPROXIMATE)

1 inch (in)	=	2.5 centimeters (cm)
1 foot (ft)	=	30 centimeters (cm)
1 yard (yd)	=	0.9 meter (m)
1 mile (mi)	=	1.6 kilometers (km)

AREA (APPROXIMATE)

1 square inch (sq in, in^2)	=	6.5 square centimeters (cm^2)
1 square foot (sq ft, ft^2)	=	0.09 square meter (m^2)
1 square yard (sq yd, yd^2)	=	0.8 square meter (m^2)
1 square mile (sq mi, mi^2)	=	2.6 square kilometers (km^2)
1 acre = 0.4 hectare (he)	=	4,000 square meters (m^2)

MASS - WEIGHT (APPROXIMATE)

1 ounce (oz)	=	28 grams (gm)
1 pound (lb)	=	0.45 kilogram (kg)
1 short ton = 2,000 pounds (lb)	=	0.9 tonne (t)

VOLUME (APPROXIMATE)

1 teaspoon (tsp)	=	5 milliliters (ml)
1 tablespoon (tbsp)	=	15 milliliters (ml)
1 fluid ounce (fl oz)	=	30 milliliters (ml)
1 cup (c)	=	0.24 liter (l)
1 pint (pt)	=	0.47 liter (l)
1 quart (qt)	=	0.96 liter (l)
1 gallon (gal)	=	3.8 liters (l)
1 cubic foot (cu ft, ft^3)	=	0.03 cubic meter (m^3)
1 cubic yard (cu yd, yd^3)	=	0.76 cubic meter (m^3)

TEMPERATURE (EXACT)

[(x-32)(5/9)] °F = y °C

METRIC TO ENGLISH

LENGTH (APPROXIMATE)

1 millimeter (mm)	=	0.04 inch (in)
1 centimeter (cm)	=	0.4 inch (in)
1 meter (m)	=	3.3 feet (ft)
1 meter (m)	=	1.1 yards (yd)
1 kilometer (km)	=	0.6 mile (mi)

AREA (APPROXIMATE)

1 square centimeter (cm^2)	=	0.16 square inch (sq in, in^2)
1 square meter (m^2)	=	1.2 square yards (sq yd, yd^2)
1 square kilometer (km^2)	=	0.4 square mile (sq mi, mi^2)
10,000 square meters (m^2)	=	1 hectare (ha) = 2.5 acres

MASS - WEIGHT (APPROXIMATE)

1 gram (gm)	=	0.036 ounce (oz)
1 kilogram (kg)	=	2.2 pounds (lb)
1 tonne (t)	=	1,000 kilograms (kg)
	=	1.1 short tons

VOLUME (APPROXIMATE)

1 milliliter (ml)	=	0.03 fluid ounce (fl oz)
1 liter (l)	=	2.1 pints (pt)
1 liter (l)	=	1.06 quarts (qt)
1 liter (l)	=	0.26 gallon (gal)
1 cubic meter (m^3)	=	36 cubic feet (cu ft, ft^3)
1 cubic meter (m^3)	=	1.3 cubic yards (cu yd, yd^3)

TEMPERATURE (EXACT)

[(9/5) y + 32] °C = x °F

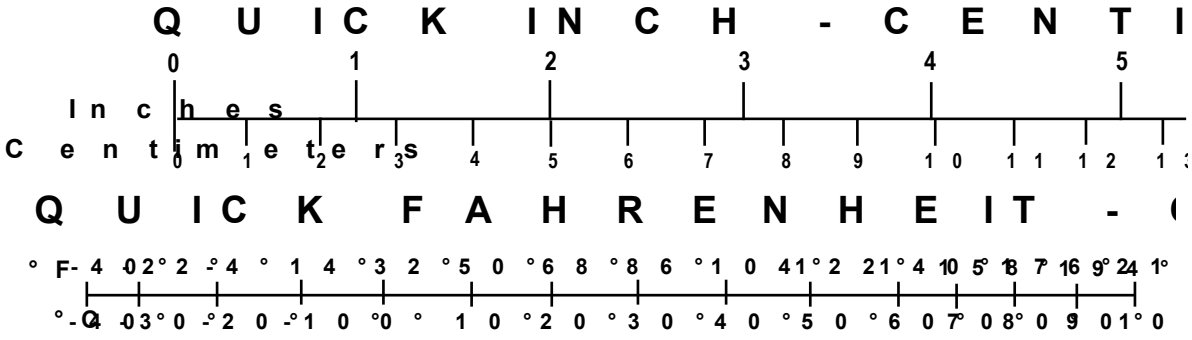

For more exact and or other conversion factors, see NIST Miscellaneous Publication 286, Units of Weights and Measures. Price $2.50 SD Catalog No. C13 10286

Updated 6/17/98

Acknowledgements

The authors would like to acknowledge the Union Pacific Railroad for providing access to track for measuring and collecting ballast samples.

Contents

Illustrations

Tables

Executive Summary

A prototype man-portable ground penetrating radar (GPR) system called the RAdar Ballast Inspection Tool (RABIT) was designed, built, and tested by Earth Science Systems, LLC (ESS) at their facility in Wheat Ridge, CO, with funding by the Federal Railroad Administration via a research proposal submitted through a Broad Agency Announcement. Testing was performed from July 2013 through December 2014 where track inspectors non-destructively assessed ballast fouling and moisture conditions. The RABIT system was successfully demonstrated using full-scale ballast models at the Union Pacific Railroad (UP) Rocky Siding track site, west of Highway 93, near Arvada, CO. Fouling and moisture content were successfully measured to ±4.7 percent and ±0.75 percent uncertainty by weight respectively. While successful, there were several recommended improvements and tests for the next phase of this project.

Due to the existing prototype weighing 63 lbs. (29 kg), as well as larger and heavier than desired, it was recommended to build a very small lightweight unit (8 lbs. or 3.6 kg) version of the RABIT that can be used for making spot measurements. There were some difficulties with making spot measurements, so it was also recommended to build a system (<50 lbs. or 23 kg) that runs on a small track dolly for making more detailed continuous measurements. The RABIT is designed primarily to measure moisture and fouling, but it is unclear as to how these properties relate to ballast strength and resiliency. Our next phase of the project includes building ballast specimens with a range of geotechnical properties and conducting tests to be able to map GPR-measured properties to mechanical properties.

This report is organized chronologically, and describes the tasks that were completed in the first year of the project, i.e., Phase I. First, there was an analysis of the fundamental relationships between electromagnetic properties and geotechnical properties, and through this it was found that GPR is significantly more sensitive to moisture than fouling. Then the physical layout of the RABIT antennas and hardware is discussed along with the reasoning for the chosen layout. Next, the full-scale ballast models that were built for conducting GPR tests with known geotechnical properties are described. Several data modeling and analysis routines were created: a full-waveform forward model, full-waveform inversions, and a method to map wave attributes to fouling and moisture. The wave attributes method provides the best results for single spot measurements. Finally, datasets were collected from the full-scale ballast models and from the UP site.

The results from the first year were encouraging, and showed that moisture and fouling could be successfully measured with non-invasive methods. The initial tests also identified shortcomings that must be addressed in future work. ESS is optimistic that a successful system can be made for ballast inspectors because several methods have been identified for making these measurements and dealing with their shortcomings.

1. Introduction

This project seeks to build, test, and demonstrate a tool for detecting ballast fouling that provides ballast condition information in real-time to track inspectors in a simple easy-to-read format. This tool, the RAdar Ballast Inspection Tool (RABIT), was built by Earth Science Systems, LLC (ESS) as a lightweight man-portable device that automatically analyzes the geophysical readings and provides fouling information directly to the operator. The RABIT makes spot measurements without taking the track out of service. It is easy-to-use, designed to have minimal controls, and requires minimal operator training.

1.1 Background

Ballast fouling is one of the primary causes of degradation of the subsurface support structure in railways. It weakens resistance to forces applied by the ties, and reduces resilient modulus and energy absorption capacity (Selig, E. T., and Waters, J. M., 1994). Previous research has shown that ground penetrating radar (GPR) is a promising technique for investigating the condition of railway ballast and subgrades (Levomaki et al., 2010) (Al-Qadi et al., 2007). The aim of this project is to expand on this previous research and provide a more quantitative assessment of ballast condition.

This project seeks to develop ballast inspection technologies that can be used by railroad track inspectors. The RABIT can make the required measurements without disturbing or removing any ballast. In accordance with the Federal Railroad Administration's (FRA) recommendations, the developed instrument aims to be highly portable and can be carried by one person. The instrument provides a percentage of fouling materials present over a unit volume of ballast. Additionally, we examined methods for estimating other useful properties of the ballast such as: ballast depth, ballast void ratio, moisture content, dielectric constant, and ballast grain size.

1.2 Objectives

The objectives of this project are identified as follows:

- To develop a multi-offset multi-frequency GPR ballast inspection instrument be built that is man-portable
- To determine the usefulness of multi-offset data and multi-frequency data
- To assess the limitations that are incurred by making spot measurements rather than continuous measurements along the track
- To determine the measurement of fouling material and moisture content
- To deduce what improvements can be made to the instrument and the analysis software, based on the results from the initial prototype
- To develop a field testing program that will demonstrate the value of the new tool and help garner adoption by the industry, based on the preliminary results
- To analyze the relationship of the properties measured by the inspection tool to other properties such as elastic modulus and yield strength to achieve industry adoption

1.3 Overall Approach

The first task was to design and build a man-portable instrument that collects GPR data at multiple frequencies and multiple offsets. The system was built using newly developed GPR technology by ESS. This system is called the RAdar Ballast Inspection Tool (RABIT).

Algorithms were created using software to simulate the response of the instrument to horizontally layered media with arbitrary layer thicknesses and properties (i.e., fouling and moisture); then inversion routines were created that attempt to estimate the properties of the layers. Useful data attributes were extracted and related to geotechnical properties.

A series of physical full-scale ballast models were built with a variety of fouling and moisture conditions. GPR data were collected on each ballast model, and geotechnical tests such as moisture and grain size distribution were conducted to provide ground truth. The modeling algorithms were also calibrated by this data.

A small survey was conducted on a Union Pacific Railroad (UP) house track where GPR measurements and a small set of samples were collected and used as an initial field test of the RABIT system.

Finally, we used the technologies, methodologies, and datasets described above to assess the system performance, draw conclusions, and determine the course of action for further research.

1.4 Scope

This project examined the viability of using ground-coupled GPR for ballast inspection. ESS intentionally did not consider air-coupled and mobile radar units that are operated from high-rail vehicles, geometry cars, and other rolling stock. The use of air-coupled GPR has been studied extensively (Levomaki et al., 2010) (Al-Qadi et al., 2007). In order to create a man-portable instrument, the array was also limited in size. A more complete picture of the ballast and sub-ballast could be obtained with an array of antennas spanning from one shoulder to the other, and possibly spanning multiple cribs. As the RABIT was designed to take 'snapshots' at one or a few locations, there was no attempt to identify locally continuous subsurface structures such as continuous layer boundaries, ballast pockets, and clay lenses.

1.5 Organization of the Report

This report covers the design and construction of the basic technologies involved in the RABIT system: GPR fundamentals, the portable GPR unit, the modeling and analysis of algorithms, construction and testing of ballast models, field testing, and the data analysis and system assessment. Section 1 through Section 5 are dedicated to these topics, and present them in chronological order that the work was completed. Section 6 summarizes the project findings, conclusions, and provides recommendations for further research.

2. GPR Background and RABIT Hardware Design

GPRs transmit temporally compact electromagnetic (EM) wavelets that travel through the media in a direct or reflected wave path, and arrive at the receiver after some delay and with some attenuation. When radar is transmitting and receiving, antenna are placed on the ground with a constant offset between them (i.e., a bi-static antenna configuration), a direct wave travels between the antennas through the air, another direct wave travels through the ground, and reflected waves occur when incident waves bounce off of contrast between EM properties in the subsurface (or above the surface). The EM properties of the media along the wave path can be deduced with knowledge of the wave path and the measured travel time and attenuation.

The travel time of an EM wave depends on the wave velocity of the medium, which in turn depends on the dielectric constant (which can be frequency dependent). The dielectric constant of ballast material depends on the type of aggregate material, the amount of fines filling the voids, and the moisture content. In a layered medium, the recorded travel time of a reflected wave using a pair of antennas (one for transmitting and the other for receiving) at a fixed offset does not provide enough information to determine both layer thickness and wave velocity. However, the travel times recorded using multiple antenna offsets do provide enough information to solve for both layer thickness and EM velocity (thus dielectric constant).

The attenuation of EM waves occurs when a medium absorbs energy (as in a microwave oven), and when the waves scatter out of the considered travel path. This scattering can be specular or diffuse. Specular scattering occurs when waves bounce off surfaces that are much larger than a wavelength (e.g., the bottom of a horizontal layer), and diffuse volume scattering occurs when the surfaces are smaller or similar to a wavelength (e.g., voids spaces between the aggregate). All waves experience wavefront spreading where the amplitude falls of as r^{-2} from the transmitting antenna (r is distance from the antenna).

GPR surveys can be conducted over a wide range of frequencies and wavelengths, but are generally performed in the 50 MHz to 2 GHz range. The EM wavelength in earth materials (i.e., minerals, rocks, soil and water) is mostly a function of moisture content. For dry earth the wavelengths at 50 MHz and 2 GHz are typically 300 cm and 7.5 cm respectively, and 120 cm and 3 cm for wet earth. At low frequencies, the penetration is good when conductivity is low, but the resolution is poor. At high frequencies, the resolution is good, but diffuse volume scattering can cause significant attenuation. Volume scattering occurs when the particle size (aggregate or voids) is similar to a wavelength. In general, there is a frequency window where GPR works well. At low frequencies, the attenuation (per wavelength) increases with increasing conductivity and decreasing frequency. At high frequencies, attenuation increases with increasing aggregate or void size and with increasing electrical contrast between the aggregate and voids. Additionally, as frequency increases above 1 GHz, the attenuation due to the dielectric relaxation of water increases. As a result, GPR surveys are commonly operated in the 50 MHz to 2 GHz window.

GPR surveys can be conducted using ground-coupled or air-coupled antennas. When the antenna is within a quarter wavelength from the ground (150 cm at 50 MHz and 3.75 cm at 2 GHz) the antennas are considered ground coupled. When the antennas are greater than a wavelength from the ground (6 m at 50 MHz and 15 cm at 2 GHz) they are considered air-coupled. When using ground-coupled antennas, the shallow ground under the antennas becomes part of the antenna, therefore, the antenna response changes as the shallow ground properties

change. Surface roughness and variable shallow ground properties affect the quality and repeatability of ground-coupled GPR measurements. Ground-coupled antennas can transmit more energy into the subsurface than air-launched antennas and subsequently they provide a greater penetration depth. Air-launched antennas have the benefit of a constant response and are better suited for use from a mobile platform such as a high-rail vehicle.

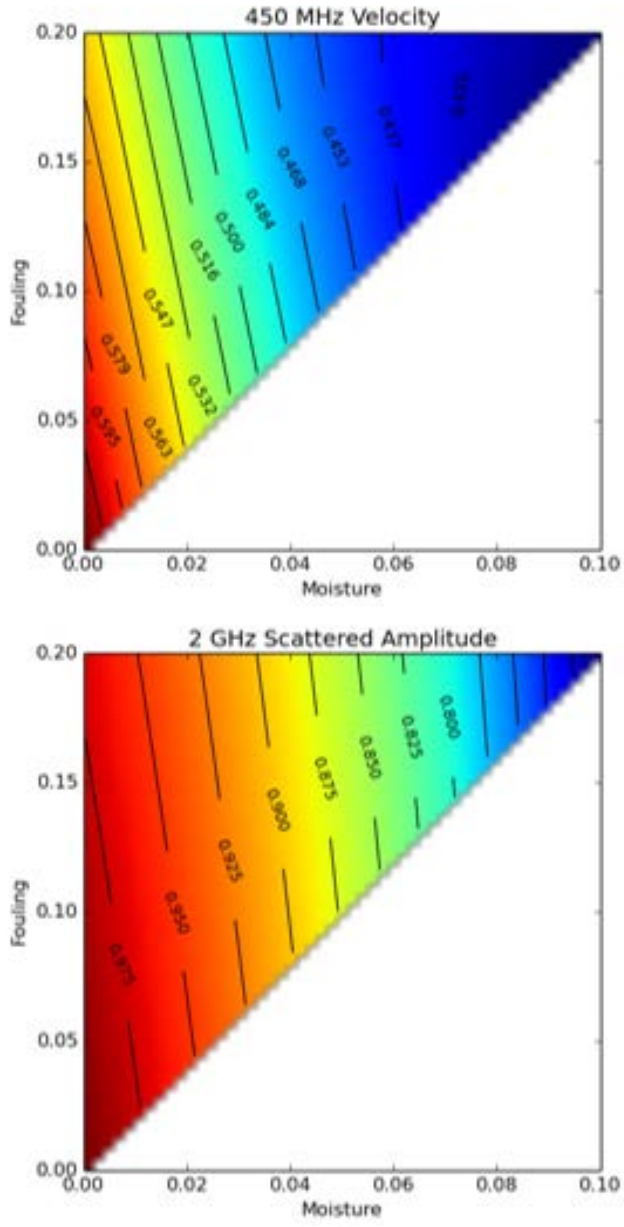

Figure 1. EM Wave Velocity and Backscatter Amplitude vs. Fouling and Moisture as Predicted by Equivalent Media Mix Law Relationships

In ballast materials, it is known that both moisture and fouling affect the propagation velocity and attenuation of EM waves. Consider Figure 1, where the 450 MHz EM wave velocity (normalized to the velocity in free space) and the 2 GHz scattered amplitude (relative to clean dry ballast) are plotted versus the volume fraction of fouling material and moisture. From the

field capacity studies described in Section 3.1.1, it is known that one part moisture requires approximately two parts fouling material to hold it in place, therefore the lower right corners of the plots are blank because this scenario cannot occur (i.e., cannot have more moisture than the ballast can hold). The plotted ranges of fouling material and moisture span the values that commonly occur in ballast. The velocity plot was calculated using the mixing laws described in Section 4. For the high-frequency scattered amplitude there are two phenomena that affect the GPR scans: volume scattering due to contrasting EM properties between the aggregate and the voids, and dielectric absorption by water. These phenomena are difficult to accurately model, so the plot shows a heuristic representation of these effects based on contrast and moisture content. Note that both EM velocity and scattered amplitude have some sensitivity to fouling material, but are most sensitive to changing moisture content. A simple velocity or scattered amplitude measurement alone does not provide enough information to assess both fouling and moisture content. Furthermore, since the contours on both plots are similar, the combination of both measurements does not provide enough information to provide reliable estimates of both fouling and moisture. These measurements provide a good indication of moisture only.

2.1 RABIT Design and Prototype

After considering the phenomena above, we concluded that the RABIT should be a dual-frequency dual-offset GPR system. This arrangement provides sufficient information for determining both thickness and propagation velocity in a horizontally layered subsurface. The low frequency measurements provide information regarding the layered geometry, and the high-frequency measurements provide information about the pore contents (air, water, and fine-grained material). Both fouling and moisture cannot be determined from wave velocity alone (see Figure 1). The additional independent back-scatter measurements from high-frequency (2 GHz) scans might provide the additional information needed to make a unique mapping between measured parameters and geotechnical parameters (i.e., fouling and moisture).

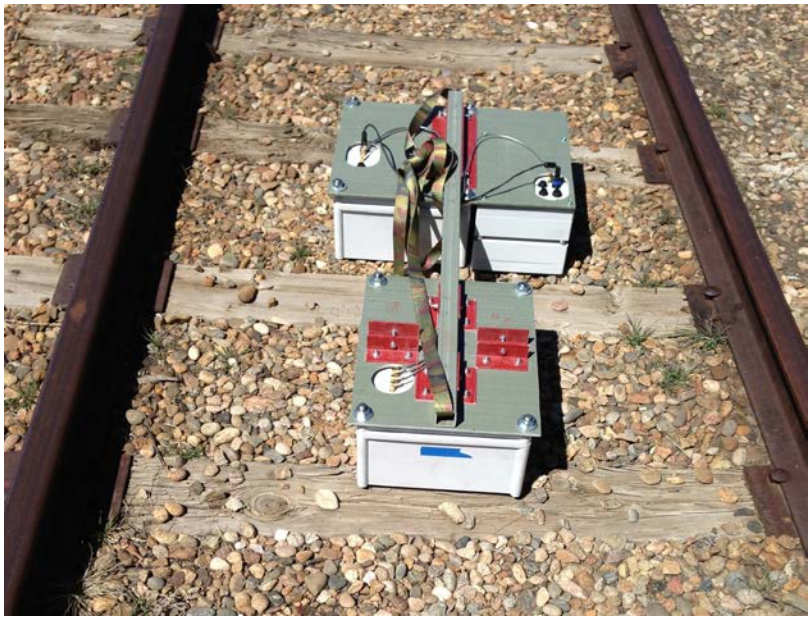

Figure 2. The Initial RABIT Configuration with Adjustable Antenna Mounting Plates to Reconfigure the Antenna Orientation and Offset

The RABIT was built using two previously designed and tested electronics and antennas. The first was a high-power 450 MHz system designed for increased penetration depth for utility detection, and the second is a fast-acquisition 2 GHz system designed for collecting high resolution data from a vehicle moving at highway speeds. For this project, we employed one of each of these systems and configured them to record multi-offset data. A common battery and charging circuit was made to power both radar systems. The initial prototype had multiple antenna mounting plates for deploying antennas in different configurations (see Figure 2). It was thought that different antenna configurations would be needed to accommodate both concrete and timber ties due to interfering reflections from the rails or rebar in the ties.

Different antenna orientations were tested on Denver area tracks with concrete and timber ties to determine if any orientations had unwanted sensitivity to the rails or ties. Results from these tests indicate that the system is relatively insensitive to interference from the rails, which is a benefit of ground coupling (and good antenna shielding). The 450 MHz measurements are very repeatable and insensitive to lateral crib position as long as the antennas are at least 4 inches (10 cm) from the rail. Due to their small wavelength, the 2 GHz measurements are very sensitive to position, and generally do not provide repeatable results. This is expected since shifting the instrument's location laterally by a few inches (or cm) from a previous location provides a significant change in the specific aggregate stones and voids that the radar waves traverse.

The initial prototype configurations were unwieldy, and because testing showed that the system is minimally sensitive to the rails, we configured the prototype so that the antennas were co-polarized with the rails and cross-polarized (i.e., minimally polarized) to the ties and any rebar they may contain. Figure 3 shows the in-line configuration that was adopted to demonstrate the capabilities of the method through subsequent laboratory and field testing. The current weight of the unit is 63 pounds (28.6 kg), so more work is needed to make the system more light-weight and portable (a future antenna design will provide significant weight and size reduction). A possible feature for a future version is a telescoping backbone so that different crib sizes can be accommodated.

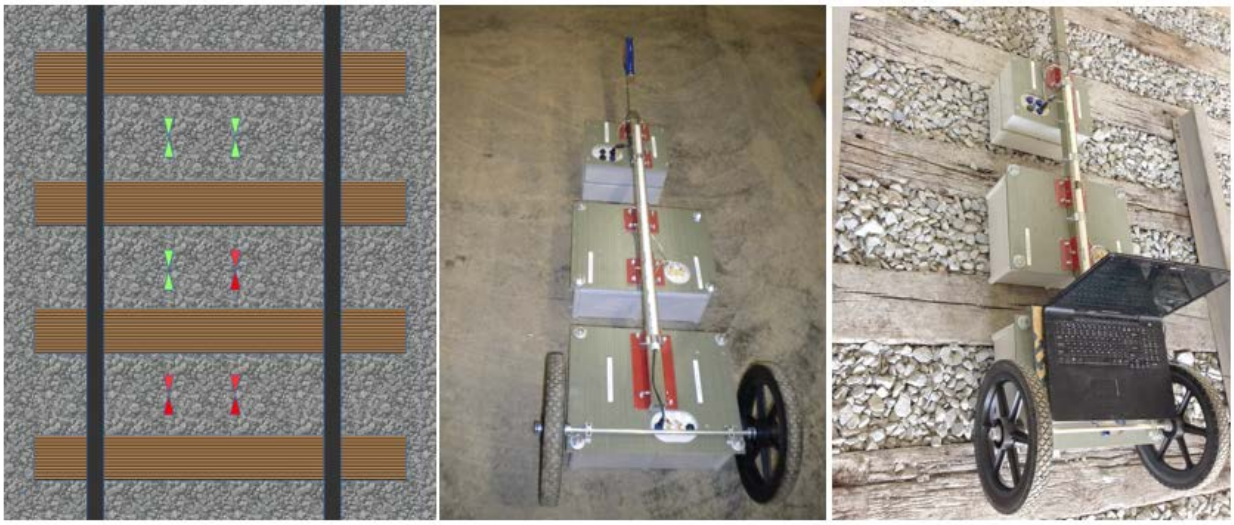

Figure 3. Left Panel Shows the Antenna Layout with the 450 MHz Antennas in Red and the 2 GHz Antennas in Green, and the Right Panels are Photos of the RABIT System

3. Ballast Models

A series of full-scale ballast models were built at the University of Massachusetts Amherst (UMass) with carefully controlled geotechnical properties in order to determine the GPR response to different fouling and moisture conditions. A schematic of the models is shown in Figure 4 and the physical construction is shown in Figure 5. The walls of the box containing the sub-ballast had internal dimensions of 17.5 × 17.5 × 1.5 ft. (5.33 × 5.33 × 0.46 m) and were made of a layer of ¾ in (19 mm) plywood supported by 2 × 4 in. (51 × 102 mm) pine lumber structure and diagonal bracing with the same pine lumber at 18 in (0.46 m) intervals. The braces were anchored in ¾ in thick plywood to prevent any lateral movement. All connections were designed to have the least possible amount of metallic components in order to prevent any unwanted reflection of the radar signals. The internal surface of the box was covered by two layers of a 6-mil plastic sheet to make the box water resistant (see Figure 5), then the box was filled with 1.5 ft. (0.46 m) clean well graded sandy sub-ballast. The sub-ballast was carefully compacted in seven layers with equal thicknesses in order to maintain relative uniformity of density. To make the GPR signal reflection from the top of the sub-ballast layer stronger, the sub-ballast layer was sprayed with water and covered with plastic to keep it moist.

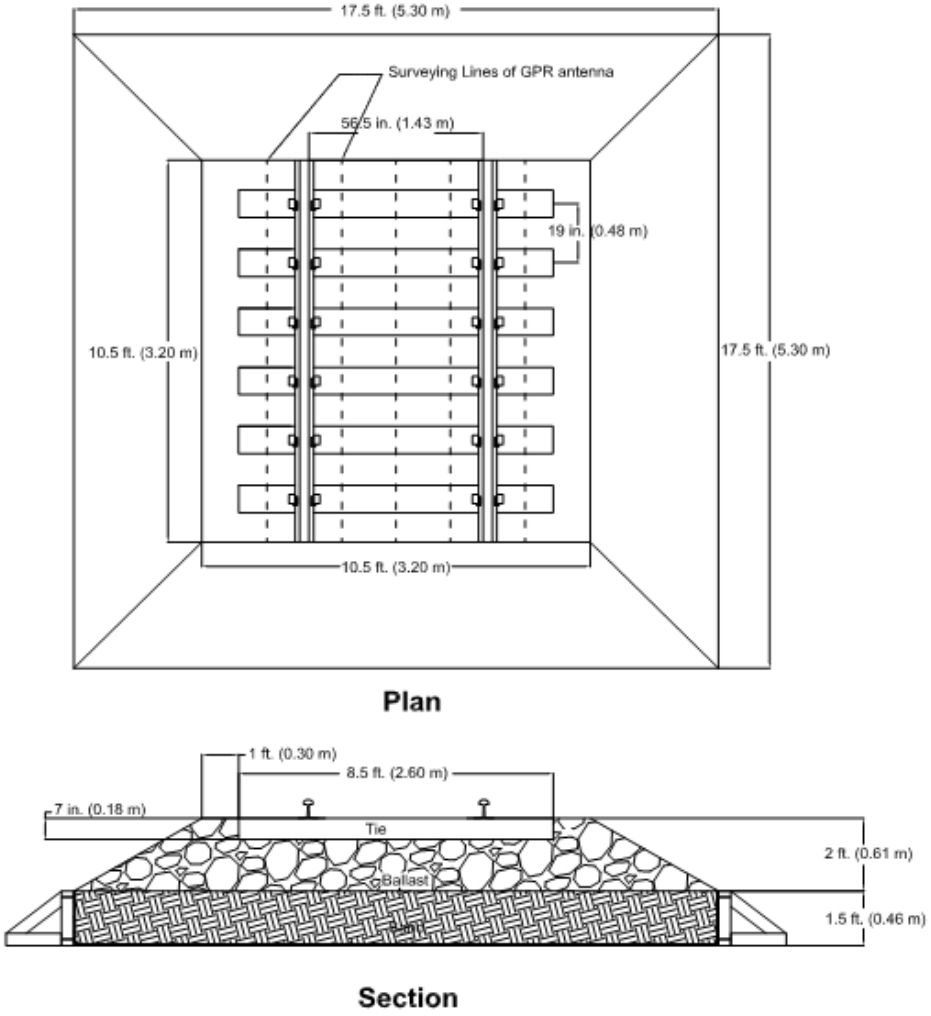

Figure 4. Schematic of Ballast Models with Plan View Above and Section View Below

The ballast was built in five lifts: three 4 in (102 mm) lifts at the bottom, followed by one 5 in (127 mm) lift, and finally one 7 in (178 mm) lift at the top. Two triangular templates were fixed to each corner of the box to control the slope on the sides of the model. The ballast used in this study was Connecticut granite meeting American Railway Engineering and Maintenance-of-Way Association #4 gradation (AREMA, 2010). Three models were built with different target fouling percentages (0, 15 and 30 percent by weight) using stone dust from the same granite source. This method creates a fouled ballast model that is similar to breakdown fouling that is most commonly observed in field situations in North America (Selig, E. T., and Waters, J. M., 1994). For each lift, a known mass of material was compacted to a target height to achieve uniform density. Lifts which had a height of 4 in (102 mm), or more were divided into two or three sub-lifts to make the spreading and hand operated compaction process more effective. To build the second and third models with 15 percent or more fouling, the pre-determined volume of fine-grained material for each layer was deposited by hand as a thin layer on each sub-lift so that the fouling could be maintained as uniform as reasonably achievable. By keeping each sub-lift thin, the fined grained material could be distributed uniformly by visual inspection. After the completion of the forth lift, the surface was leveled accurately prior to the installation of the timber ties. The fifth lift filled the crib space up to the top surface of the ties. The ties spacing was 19.5 in (495 mm) and then the rails were placed on the ties with standard North American rail gage of 56.5 in (1.43 m) (Selig, E. T., and Waters, J. M., 1994).

Figure 5. Photos Showing the Construction of a Ballast Model with the Lined Box for the Sub-Ballast (top left), Filled Sub-Ballast Box (Top Right), Filled and Lined Sub-Ballast (Bottom Left), and Complete Model (Bottom Right)

3.1.1 Wetting the Ballast Models

Each of the three ballast models was subjected to a phased irrigation procedure to produce different moisture levels. To determine how much moisture was needed to reach a target level, the field capacity of the dry ballast was experimentally determined. Then the required volume of water needed to reach the target moisture level was calculated as a percentage of field capacity, and this water was used to irrigate the model using the apparatus shown in Figure 6. This irrigation fixture was built from a perforated PVC pipe, and the entire assembly was rotated by hand during irrigation in order to distribute the moisture as uniformly as reasonably achievable. After irrigation, the model was covered with a plastic sheet for 24 hours to let the water come to an equilibrium distribution.

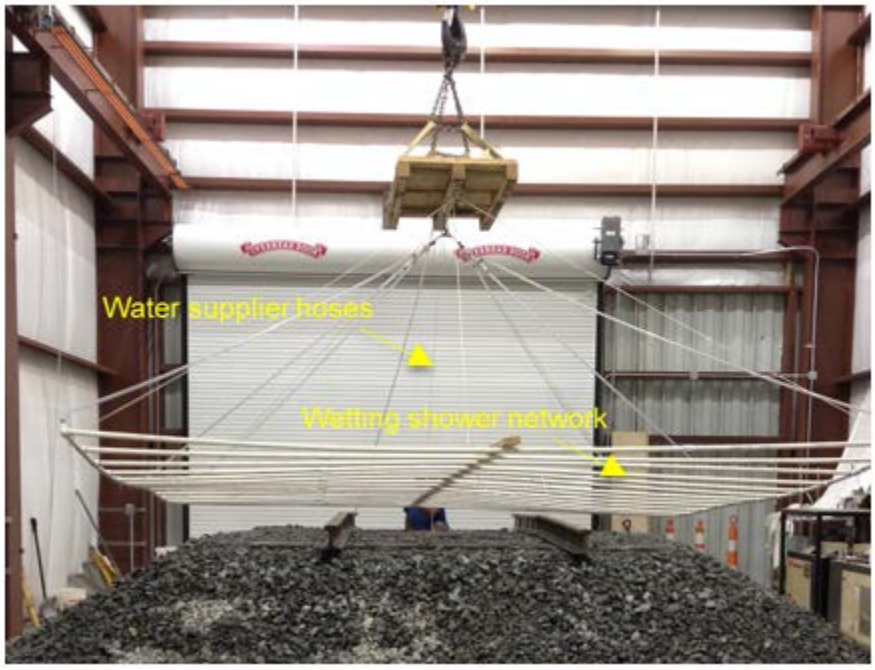

Figure 6. Apparatus Used to Wet the Models. Water Was Supplied to a Grid of Perforated PVC Pipe Via a Network of Feeder Hoses

To determine the field capacity, three small (~2 liter) ballast specimens for each full-scale model were created with the same grain-size distribution (GSD) and fouling percentage used in the full-scale models. The small specimens were then immersed in water for 24 hours and then allowed to drain. Five samples were taken from each specimen for determining water content using the ASTM D2216-05 standard procedure (ASTM, 2007). The measured field capacities for the specimen with 0 percent fouling were quite repeatable (i.e., the standard deviation was 0.04 percent), and the mean value was used as the representative field capacity. For the 15 percent and 30 percent fouled models, the fine-grained material migrated towards the bottom of the reconstituted specimen during the draining process. This resulted in a non-uniform fouling and moisture profile. In order to obtain a useful relationship between fouling and field capacity, each sample was passed through a 3/8 in. (9.5 mm) sieve to separate the fouling material from the course grained material (a single sieve was adequate for separating the fouling material because the specimens were gap-graded [Selig, E. T., and Waters, J. M., 1994]). The separated samples were then weighed and the results used to plot fouling versus moisture (by weight) for the

reconstituted specimens. Figure 7 shows these relationships for the 15 percent and 30 percent fouled reconstituted specimens. Table 1 shows the target moisture values that were used to irrigate the full-scale models. These moisture values linearly increase from zero to field capacity. For the 15 and 30 percent models, the field capacity was determined using the known fouling percentage (red circles) and the graphs in Figure 7.

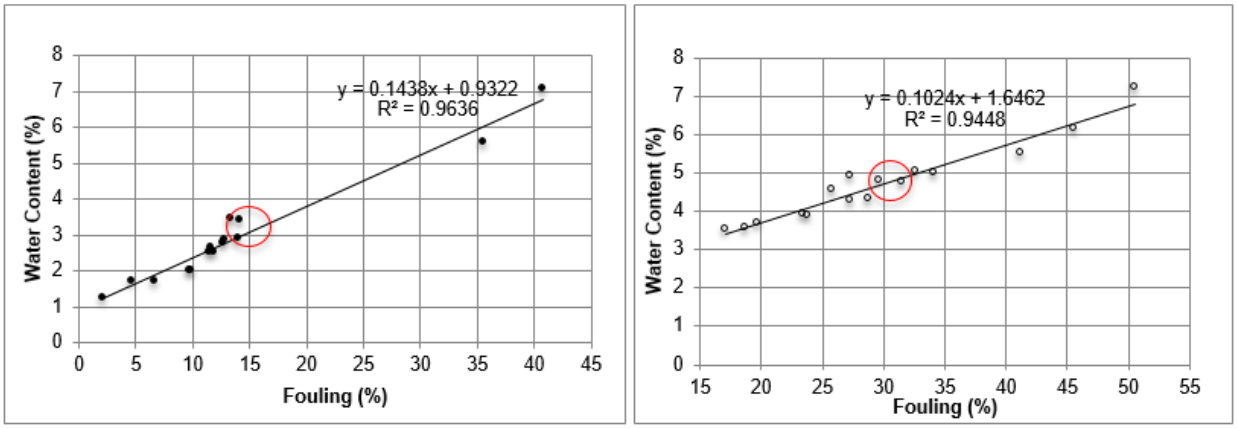

Figure 7. Experimentally Determined Field Capacity vs. Fouling for the 15 Percent and 30 Percent Fouled Models (Left and Right Respectively)

3.1.2 Measuring the Geotechnical Properties of Ballast Models

After building each ballast model, each of the three ballast models was subjected to a four-step irrigation process to obtain the four different target moisture levels listed in Table 1. After irrigation, the ballast models were covered with a plastic sheet for 24 hours to allow the moisture to reach an equilibrium distribution. GPR surveys were then taken for each moisture level on each ballast model. After collecting the GPR data, samples were taken from each ballast model and used to determine the actual density, moisture content, and GSD.

Table 1. Target Moisture Values for Ballast Models

	0% Model	15% Model	30% Model
Dry[1]	0	0	0
w_1[1]	0.26	1.07	1.6
w_2[1]	0.52	2.14	3.2
Field Capacity[1]	0.77	3.2	4.8

[1] Percent by weight.

Table 2. Actual Moisture Values Determined from Samples Taken from the Ballast Models

	0% Model	15% Model	30% Model
Actual Fouling[1]	1.30	14.90	27.15
Dry[1]	0.11	0.26	0.58
w_1[1]	0.45	1.59	3.48
w_2[1]	0.51	2.12	4
Field Capacity[1]	0.61	3.43	4.62

[1] Percent by weight.

The sampling process followed the method outlined in (Chen et al., 1978). After removing the sample, the sample void was lined with a plastic sheet and the void was filled with water until full. The volume of water needed to fill the void is equal to the volume of the sample. The samples were weighed before and after drying to determine moisture content in accordance to ASTM D2216-05, and the results are listed in Table 2 (ASTM, 2007). The dry samples were then sieved to determine the GSD in accordance with ASTM D6913-04 (ASTM, 2008). The results are shown in Figure 8 and listed in Table 3. Where G_s is the specific gravity, e is the void ratio, D_{10}, D_{30}, D_{50}, D_{60} are the diameters of the grains at 10, 30, 50 and 60 percent sieve passing, respectively. Cu and Cc are the coefficients of uniformity and curvature, respectively.

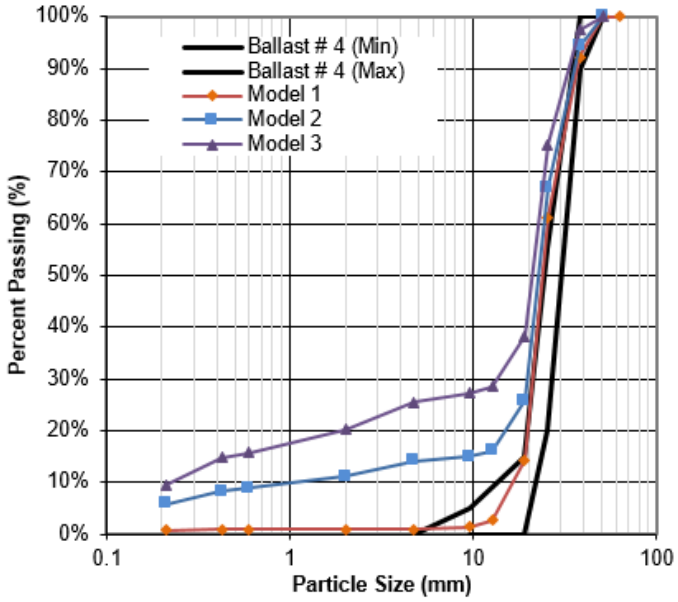

Figure 8. Experimentally Determined GSD for Ballast Models

Table 3. Sample Weights, Densities, and GSD

	0% Model	15% Model	30% Model
Fouling[1]	1.30	14.90	27.15
Specimen weight (kg)	129	171	192
Specific gravity G_s	2.75	2.75	2.75
Dry density[2] (kg/m^3)	1586 (93.3)	1940 (62.8)	2100 (72.9)
Void ratio[1] e	0.74 (0.1)	0.42 (0.04)	0.31 (0.05)
D_{10} (mm)	16.7	1.2	0.23
D_{30} (mm)	21.2	19.5	13
D_{50} (mm)	24	22.7	21
D_{60} (mm)	25.2	24.2	23
Cu (mm)	1.5	20.2	100
Cc (mm)	1.1	13.1	31.9

[1] Percent by weight.
[2] The number of tested samples collected from models based on minimum requirement for mass of test specimen under the ASTM D2216-05 standard. The number of samples tested for 0% Model, 15% Model, and 30% Model are 6, 8, and 7 respectively.

3.1.3 GPR Data Collection

Prior to conducting the destructive sample collection processes described above, GPR surveys were made for each moisture level on each ballast model. To assess whether the position of the RABIT affects the repeatability of the measurement, data were taken in three different locations on each of the five lines shown in Figure 4. This resulted in 15 datasets taken for each of the 12 fouling-moisture combinations (3 different fouling values and 4 different moisture values). To collect the data, the RABIT was placed longitudinally such that the antennas were placed over the cribs as shown in Figure 3. For the 450 MHz GPR, waveforms were collected using two adjacent antennas offset horizontally in the same crib, and using two antenna offset vertically in adjacent cribs (see left panel of Figure 3). An analogous set of waveforms was collected with the 2 GHz system.

4. Analysis Algorithms

A forward modeling algorithm was created to simulate EM wave propagation in the subsurface. The algorithm accounts for frequency dependent material properties in a layered subsurface. Inversion routines were also developed that iteratively run forward models until the modeled waveforms matches the measured waveforms. When a close match is found, the model parameters (e.g., moisture content, fouling, layer thickness, etc.) are said to represent the actual subsurface properties. The forward modeling routines are executed many times during the inversion process, so it is important that the forward model be computationally efficient.

The first step in the modeling process is to calculate the frequency dependent propagation and attenuation constants for each material. These constants specify how long it takes for a wave to travel through a layer and how much attenuation will occur. These constants are in turn a function of the EM properties of the media: the electrical conductivity, the complex frequency dependent dielectric permittivity, and the magnetic permeability (which is assumed to be that of free space). These EM properties in turn can be related to the volumetric fractions of the material's constituents. For example, if the volumetric fractions of granite, water, and air are known, and the EM properties of these constituents are known, then the resulting EM properties of the medium can be estimated using 'mixing' formulas. These estimates are often termed the 'effective' EM properties.

There are many mixing formulas that have been theoretically derived or empirically determined, and each formula makes a series of assumptions. The Bruggeman mixing formula is widely used in electromagnetics, and models each constituent as spherical inclusions in a background medium with the effective EM properties (Sihvola, A. H., 1999). There are extensions to the Bruggeman formula for ellipsoidal inclusions (e.g., disk-like or rod-like inclusions), but the assumption of spherical grains provides good results for most granular media. The Bruggeman formula is a transcendental function that must be solved iteratively. A few alternate mixing formulas were tested, but the Bruggemean formula provided the best combination of being broadly applicable and relatively efficient to calculate. To apply the Bruggeman formula, the EM properties of the subsurface constituents are needed. Table 4 lists the properties that were used in this project. The dielectric properties of air and granite are purely real and not frequency dependent, so changing the proportion of these constituents results in the same change in wave velocity for all frequencies. In contrast, the dielectric properties of water are both dispersive (i.e., the value changes with frequency) and complex (i.e., has real and imaginary values). The real and imaginary values of the relative permittivity of water are shown in Figure 9 (Hufford et al, 1991). Note that at 2 GHz, the relative imaginary permeability of water is about 10, which causes attenuation of EM waves at these frequencies. For frequencies less than about 2 GHz, the real permittivity does not change significantly, so the velocity is not frequency dependent for GPR frequencies.

Table 4. EM Properties of Subsurface Constituents

Constituent	Conductivity	Relative Dielectric Permittivity	Relative Magnetic Permeability
Air	0	1.0	1.0
Water	0	Dispersive complex values	1.0
Granite	0	4.0	1.0

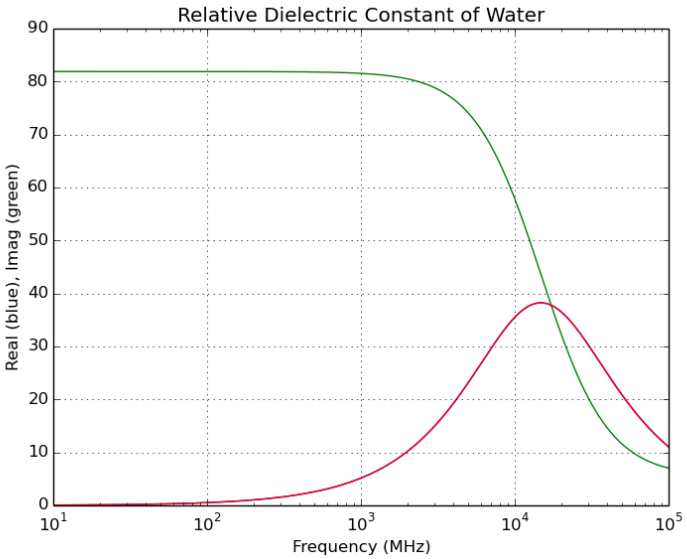

Figure 9. Dielectric Properties of Water

The previously discussed mixing laws are valid when the particle size is much smaller than a wavelength. When the particles in the random media approach the size of the EM wavelength, scattering occurs that must be accounted for. With random scattering, some of the wave energy is scattered out of the wave's propagation path, and some energy can sometimes be scattered back into the propagation path. Rayleigh scattering occurs when the scatterers are significantly smaller than a wavelength and Mie scattering occurs when the particles have a similar size to a wavelength. In these cases, the particles generally are too small to be 'imaged' by the radar survey, but can cause noisy or speckled data. When the scatterers are much larger than a wavelength, then specular reflections occur that can be used to create 'images' of the reflectors. There are several approaches to modeling random volume scattering, and they can be quite computationally demanding. Our approach is simply to model the volume scattering in a layer as a random sequence of thin layers with similar thicknesses to the ballast voids, and with slightly different properties than the effective properties. This computationally efficient approach has been used successfully by Tsang and Kong (2001). It is possible to account for GSD, particle

shape, and orientation, but this makes the calculations much more complex than necessary, and computationally inefficient.

4.1.1 Forward Modeling Algorithms

The forward modeling algorithms created for this project collect the model parameters using the input dialog shown in Figure 10. In the upper table, users enter the parameters that describe the GPR system's number of channels, antenna frequencies, antenna offsets, etc. The lower table is used to enter the geotechnical properties describing the layered subsurface: number of layers, porosity, fouling, moisture content, void diameter, etc. Using these parameters, the forward modeling algorithm follows the steps listed below to generate simulated waveforms.

1. Using the geotechnical properties for each layer and mixing rules to calculate EM properties. Then calculate the propagation and attenuation constants for each layer.
2. Calculate incident waveforms produced by each transmitting antenna.
3. Calculate the reflected ray paths for each reflector using layer thicknesses and EM properties (see Figure 11). It is necessary to solve a non-linear optimization problem to determine the propagation path lengths in each layer.
4. Follow each ray path and propagate waveforms though each layer. Calculations are conducted in the frequency domain, and propagation through each layer results in a frequency dependent phase shift and attenuation. Properly account for frequency dependent transmission and/or reflection at each layer boundary. This procedure calculates the specular response of a layered subsurface.
5. For each layer, add the volume scattering response due to small scatterers (i.e., voids in ballast). The response to these scatterers is modeled as a random sequence of thin layers with random variations in EM properties. The mean thin layer thickness is determined by the void diameter entered as a geotechnical property.

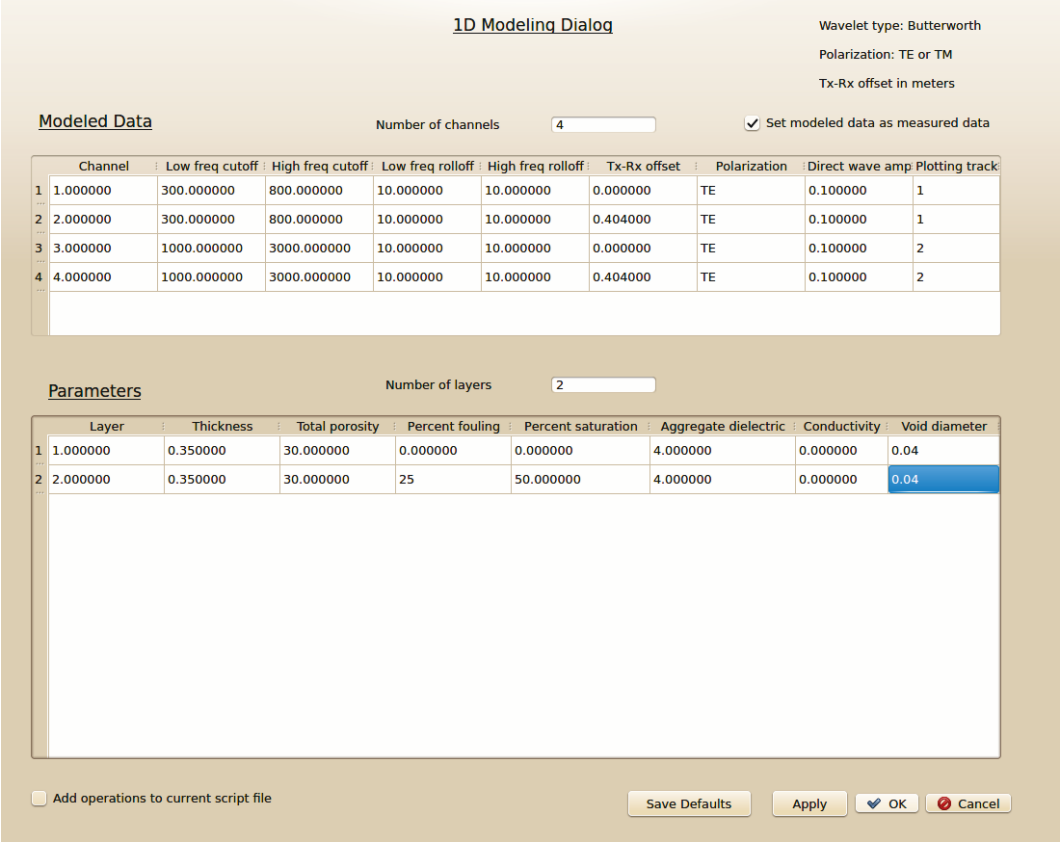

Figure 10. Input Dialog for Forward Modeling

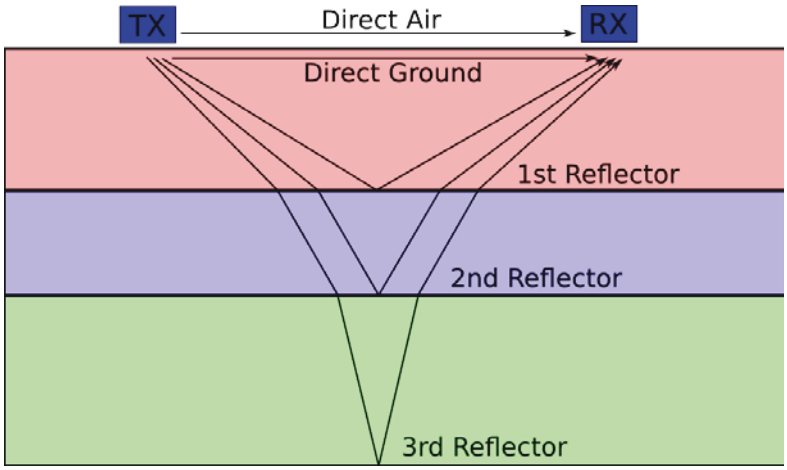

Figure 11. Ray Paths for Waves for a GPR Survey in Layered Media

An example of the resulting simulated waves for a two-layer medium can be seen in Figure 12. These waveforms show the incident or transmitted waveform and the smaller reflected waves at later times (near 5 and 10 ns). No range gain has been applied to the plots. In the 450 MHz plots, we see two reflections from each interface with different arrival times as we would expect for two different antenna offsets. The 2 GHz waveforms show the effects of volume scattering as expected (the random thin layers have little effect on the 450 MHz waveforms). The

algorithm has been tested with up to five layers, and has the ability to simulate many more layers. The direct waves are not included in the simulation at this time.

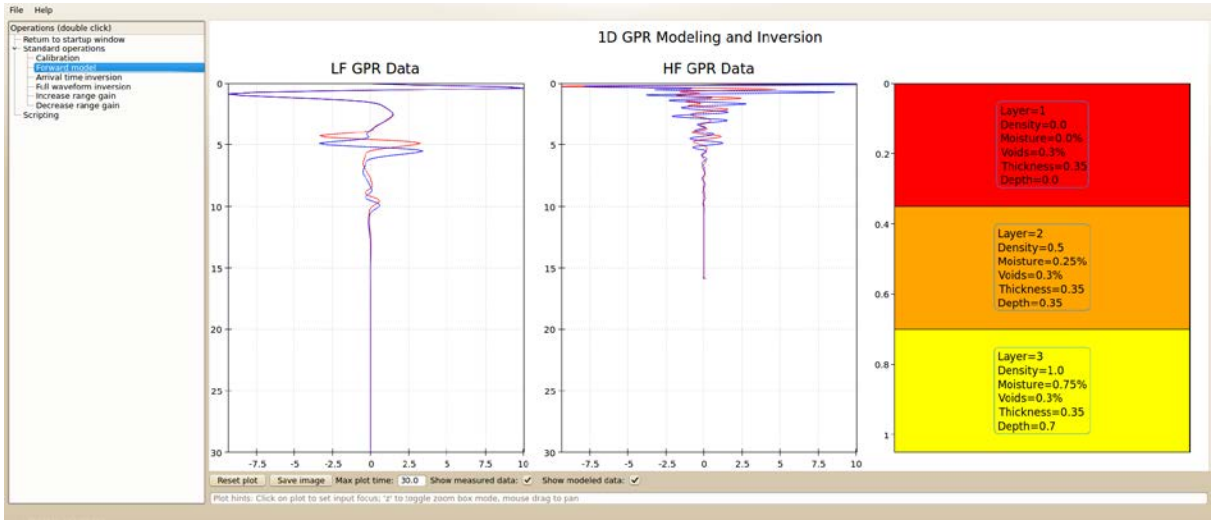

Figure 12. Plots of Modeled Data with a Two Reflecting Interfaces

4.1.2 Inversion Algorithms

Work on the inversion algorithms began after a robust forward modeling algorithm had been created. Two inversion routines were created: specular and full waveform. The specular routine for a layered subsurface uses the 450 MHz data and attempts to determine layer thickness and EM velocity for each layer. Then the full waveform routine uses these results as constraints, and attempts to match the 450 MHz reflected wavelets and the Hilbert envelope of the 2 GHz data.

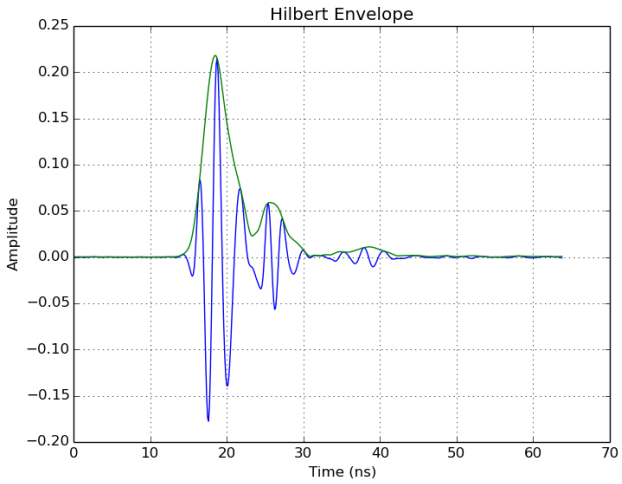

Figure 13. Hilbert Envelope of a Waveform

The steps in the specular inversion routine algorithm are listed below:

1. Calculate the Hilbert envelope of the recorded 450 MHz waveforms (see Figure 13). This produces a waveform with positive peaks that correspond to the peak energy arrival of arriving wavelets.

2. Use a wavelet domain peak picking algorithms to pick peaks and ignore noise. Since most real waveforms contain a plurality of large and small reflectors, this will produce a list of arrival times, many of which are due to unwanted reflections or noise.
3. Extract the arrival times of the largest reflected waves according to the user supplied number of layers. Repeat for the far offset channel, but with the added constraint that each far arrival time must occur later in time than the corresponding near arrival time.
4. Model the travel times for the reflection path of each layer boundary. The parameters of this model are the layer thicknesses and EM velocities for each layer. Running this model involves solving a non-linear optimization problem to determine the reflected ray paths for each reflector in a manner similar to step 3 in the forward modeling algorithm above (see Figure 11).
5. Using the extracted reflected arrival times, invert the travel-time model from the previous step to estimate layer thicknesses and velocities.

Figure 14 shows the results of the specular inversion routine, where layer thickness and velocity estimates are given. After the layer thicknesses and travel times are known, it is a straightforward matter to determine the layer's dielectric constants. After repeated testing of this routine on synthetic data, it was concluded that sensitivity to the extracted arrival times was reasonable. For example, a one nanosecond change in the arrival times for a 40-cm thick layer caused the estimated layer thicknesses to change by about 5 cm and velocities by about 8 percent; and an 8 percent variation in velocity corresponds to about an 8 percent variation in moisture. However, with field data there can be noise and clutter that makes it difficult to precisely extract arrival times, and variations of several nanoseconds are common. These variations occur due to variable coupling of ground-coupled antennas and interference from clutter and noise. When only examining a single trace from a single location, geologic noise (i.e., localized variations in material properties) is often problematic. Due to the variability in the field data (see Section 5.1.1), the specular inversion results on the field data have not been promising. Changing the geometry of the antennas or adding more offsets may make the specular inversion routine more tolerant to variations in field data, but the physical constraints of track geometry and limited signal strength at longer offsets preclude using other geometries. We recommend collecting and averaging a large number of traces in a continuous scan across the crib or along multiple cribs so that the unwanted effects of clutter and localized variations are minimized. This in fact, is the procedure employed in traditional GPR scans along a line, and is done automatically in many commercial systems.

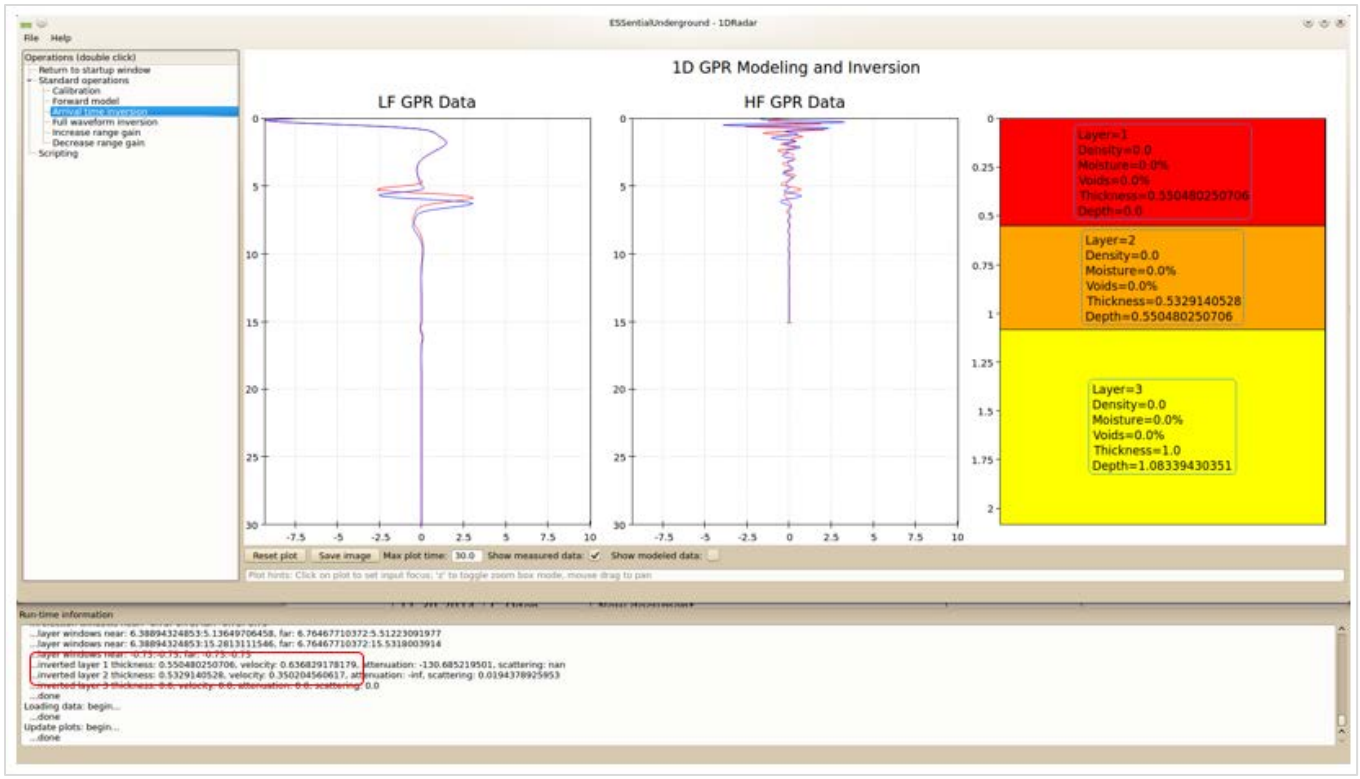

Figure 14. Specular Inversion Results for a Two Layer Model

A full waveform inversion routine was written to invert both the 450 MHz and 2 GHz GPR data using the forward model described in Section 4.1.1. This routine attempts to estimate the layer specific geotechnical properties (fouling, saturation, and void diameter) by modeling and matching the reflected wavelets from the 450 MHz data and the Hilbert envelopes of the 2 GHz data. The procedure is outlined below:

1. Using the arrival times determined from the specular inversion routine, determine the time-domain windows containing the reflected wavelets for each layer boundary. Determine the time-domain windows between reflections that contain the volume scattering response.
2. Iteratively run the full-wave forward model and attempt to determine the geotechnical properties of the subsurface layers. Measure the misfit between the modeled data and the recorded data, and use a non-linear minimization scheme to vary the geotechnical parameters to attempt to match the modeled and measured data.

Full waveform inversion is a difficult problem (and historically computationally intensive). The approach here has been to use the specular inversion to provide results that constrain the full waveform inversion to make this problem easier to solve. Even still, the current routines do not yet reliably converge with synthetic data. Due to these routines requiring accurate results from the specular routine for proper operation, and because the specular routine is not performing well with field data, this algorithm was not further developed under this project. Instead, ESS focused on extracting meaningful information from the field data that were acquired using attributes of the recorded waveforms. Note that in addition to improving the convergence issues, further

work also needs to be done in predicting source wavelet changes due to variable loading of the ground-coupled antennas.

4.1.3 Direct Wave Attributes

As the reflected wave inversions were not providing robust results with noisy field data, waveform attributes were used as indicators of the geotechnical parameters (fouling and moisture). A multi-variate second order polynomial fit was made between each attribute and fouling and moisture content. After visually examining plots of the data collected on the ballast models (see Section 5.1.1), it was determined that the eight waveform attributes listed below appeared to correlate with increasing moisture:

1. Direct wave peak amplitude from the 450 MHz near antenna offset.
2. Direct wave arrival time from the 450 MHz near antenna offset.
3. The high to low frequency spectral ratio for the direct wave from the 450 MHz near antenna offset.
4. Direct wave peak amplitude from the 450 MHz far antenna offset.
5. Direct wave arrival time from the 450 MHz far antenna offset.
6. The high to low frequency spectral ratio for the direct wave from the 450 MHz far antenna offset. This ratio is formed as described above.
7. The average amplitude of the Hilbert envelope of the 2 GHz near antenna offset.
8. The average amplitude of the Hilbert envelope of the 2 GHz far antenna offset.

These attributes can be easily extracted from the recorded waveforms even when the waveforms are noisy. Based on the theory presented in Section 2, we would generally expect these attributes to change monotonically with fouling and moisture. However, in a few cases, simply fitting a second order equation did not produce a monotonic relationship. Therefore, a monotonic constraint was added so that the fitting routine tried to produce a second order monotonic model to map the attribute to fouling and moisture values (by weight). Finally, the property estimates determined from each attribute were combined in a weighted average (by goodness of fit) to provide a joint estimate. The results (presented in Section 5.1.2) show that each independent variable provides valuable information, but the combination of these variables provides more robust estimates of fouling and moisture. Most of the attribute maps have R^2 goodness of fit values between about 0.5 and 0.8 for fouling and moisture.

5. Data Analysis

As discussed above in Section 3.1.3, a large amount of data was collected from the ballast models. The first processing step was to perform a calibration to determine time zero for the GPR systems. Calibration is necessary for proper data analysis. Collecting data for the temporal calibration was a simple matter of placing the RABIT system at a series of known distances from a high quality planar reflector and recording data. Figure 15 shows the RABIT setup in front of a metal door. Using the measured arrival time for the reflections off the metal door and the known distances from the door, the offset time for each of the four traces was determined. After calibrating, zero-time represents the time when the wavelet is leaving the transmitting antenna. There are small variations in zero-time when using ground-coupled antennas because the antenna response changes with the EM properties of the shallow ground just under the antennas. To date, we have not accounted for these small variations. A more simple calibration procedure can be used in field conditions.

Figure 15. Calibrating the RABIT by Collecting Data a Various Distances from a Planar Reflector

5.1.1 GPR Data from the Ballast Models

As mentioned previously, GPR data were taken from three positions along either 3 or 5 lines for each ballast model (see Figure 4). Figure 16 through Figure 18 shows the 450 MHz GPR data from each ballast model for the three fouling conditions at both dry and field capacity moisture levels. Figure 19 through Figure 21 shows the Hilbert envelopes of the 2 GHz GPR data over the same conditions as the 450 MHz data. Since coherent arrivals are not expected in the 2 GHz data, the envelopes are plotted for clarity. In these figures, all traces for a given fouling-moisture condition are plotted on the same graph, and the only difference between the traces is the location of the RABIT system. The thicker black trace on each plot is the average trace over all

RABIT locations. No range gain has been applied to the data, so that true amplitudes are displayed. There are several observations that can be drawn from these plots, such as:

1. Consistent changes in the data that correlate with the location across different ballast model conditions were focused on, (fouling and moisture) and no consistent behavior with any specific locations were identified.
2. The traces are quite repeatable with dry unfouled ballast. The addition of dry fouling material increases the variability with location, and the addition of moisture causes much more variability from location to location. Traces from the far offsets (antennas in adjacent cribs) have more variability with location than traces from the near offsets (antennas in the same crib).
3. When adding fouling material to each lift, the fouling material distribution was visually controlled for uniformity. This is a subjective process, so there is likely some degree of and spatial variability.
4. When adding moisture to the ballast samples that were created for assessing field capacity, the fine-grained materials migrated towards the bottom of the sample. It follows that a similar migration of fines can be expected in the full-scale ballast models resulting in non-uniformity in both fouling and moisture distributions after the water was added. In the geophysics industry, this non-uniformity is referred to as 'geologic noise.'
5. Significant geologic noise (unwanted response to local heterogeneity) is evident in these datasets—especially those with moisture present. These interfering reflections cause difficulties with automated algorithms for picking out arriving wavelets.
6. The reflected wave from the bottom of the ballast (blue arrows) moves to later times after adding moisture as expected.
7. The reflected wave from the bottom of the sand layer (red arrows) also moves to a later time after adding moisture as expected.
8. Note that the amplitude of the reflected waves changes between different fouling-moisture conditions. These amplitude changes reflect the different contrasts in EM properties between the ballast and the sand at different times, with most of the contrast provided by moisture variations. For the 0-percent fouled model, the sand subgrade was moistened but not saturated. For the 15 percent and 30 percent models, much more water was added to the sand layer before building the overlying ballast layers. The goal was to provide more electrical contrast to obtain better reflections. However, at the 5 percent moisture level in the ballast, both the ballast and the sand had a significant amount of moisture and there may not have been a large contrast. This could explain the weak sand bottom reflection for the model with 30 percent fouling and 5 percent moisture.
9. The large amount of variability in the traces reduces confidence that any one or two traces properly reflect the representative subsurface conditions. Additionally, for analysis algorithms that require accurate arrival times, these ground-coupled surveys may not be the best approach. At a minimum of ~10 traces at different locations are needed to obtain a representative trace. At a given location, successive traces are quite similar but may be responding to local heterogeneity.

10. For the 2 GHz near offset, the amplitude of the waveforms decreases with increasing moisture. This is also evident with the 2 GHz far offset to a lesser degree.
11. For the 450 MHz data, there is a small increase in the arrival time of the direct waves with increasing moisture for both the near and far offset.
12. There is a shape change in the 450 MHz direct arriving wavelet for the both offsets (most pronounced in the near offset) as moisture increases. After further investigation, it was determined that attenuation of the high frequencies is the cause of the wavelet's shape change. In the frequency domain, the phase does not change much with moisture.

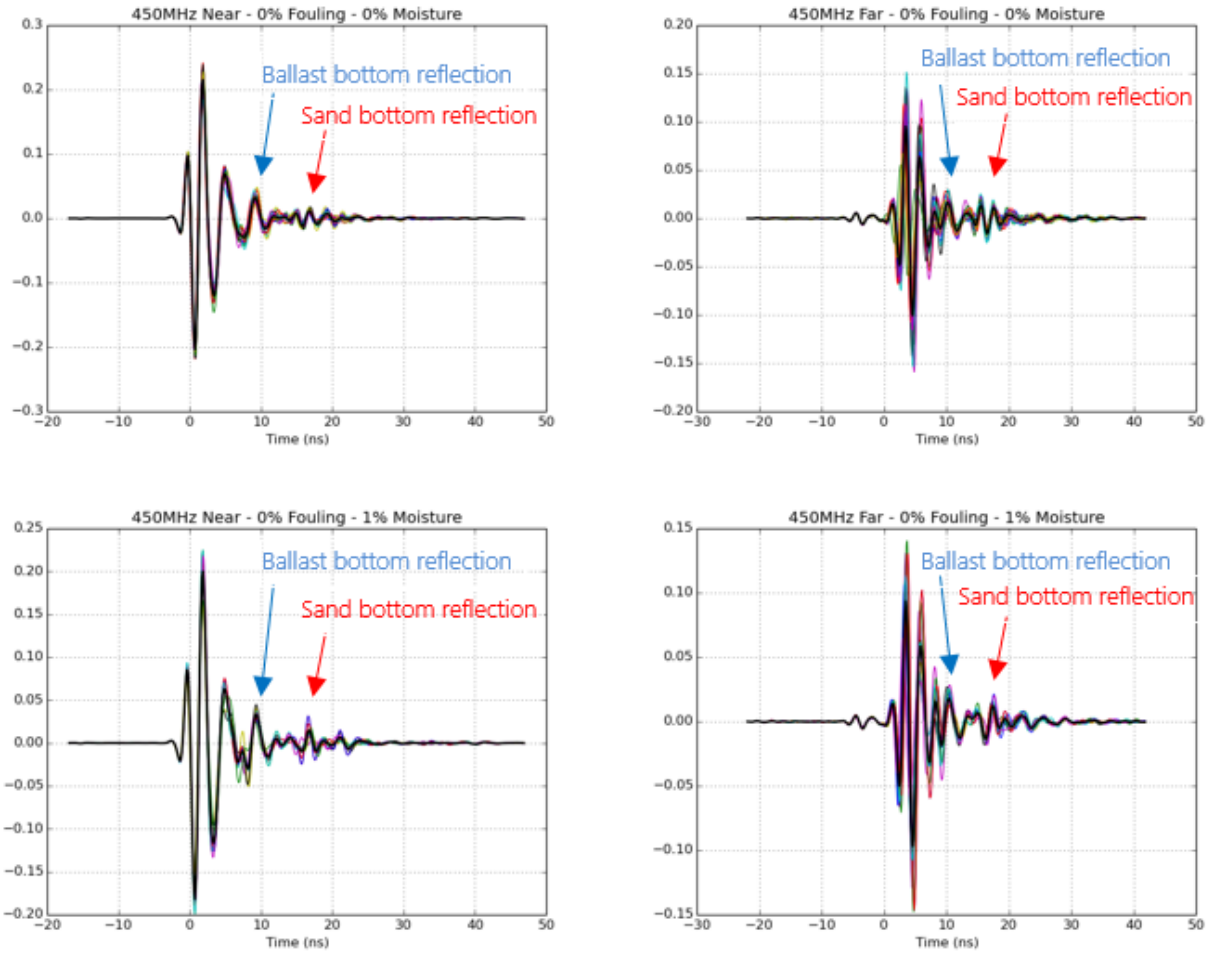

Figure 16. 450 MHz GPR Traces for the 0 Percent Fouled Ballast Model: Dry and Field Capacity

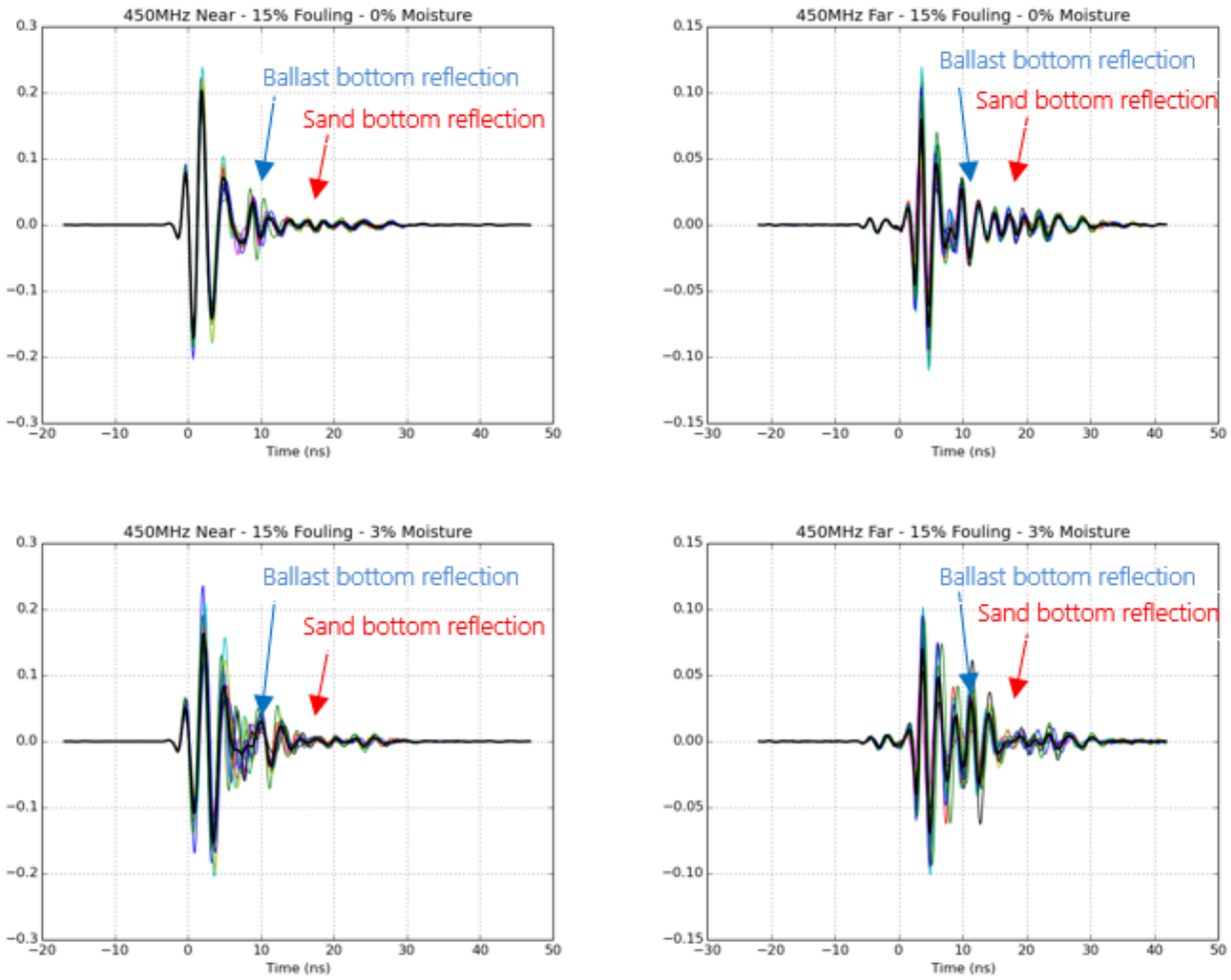

Figure 17. 450 MHz GPR Traces for the 15 Percent Fouled Ballast Model: Dry and Field Capacity

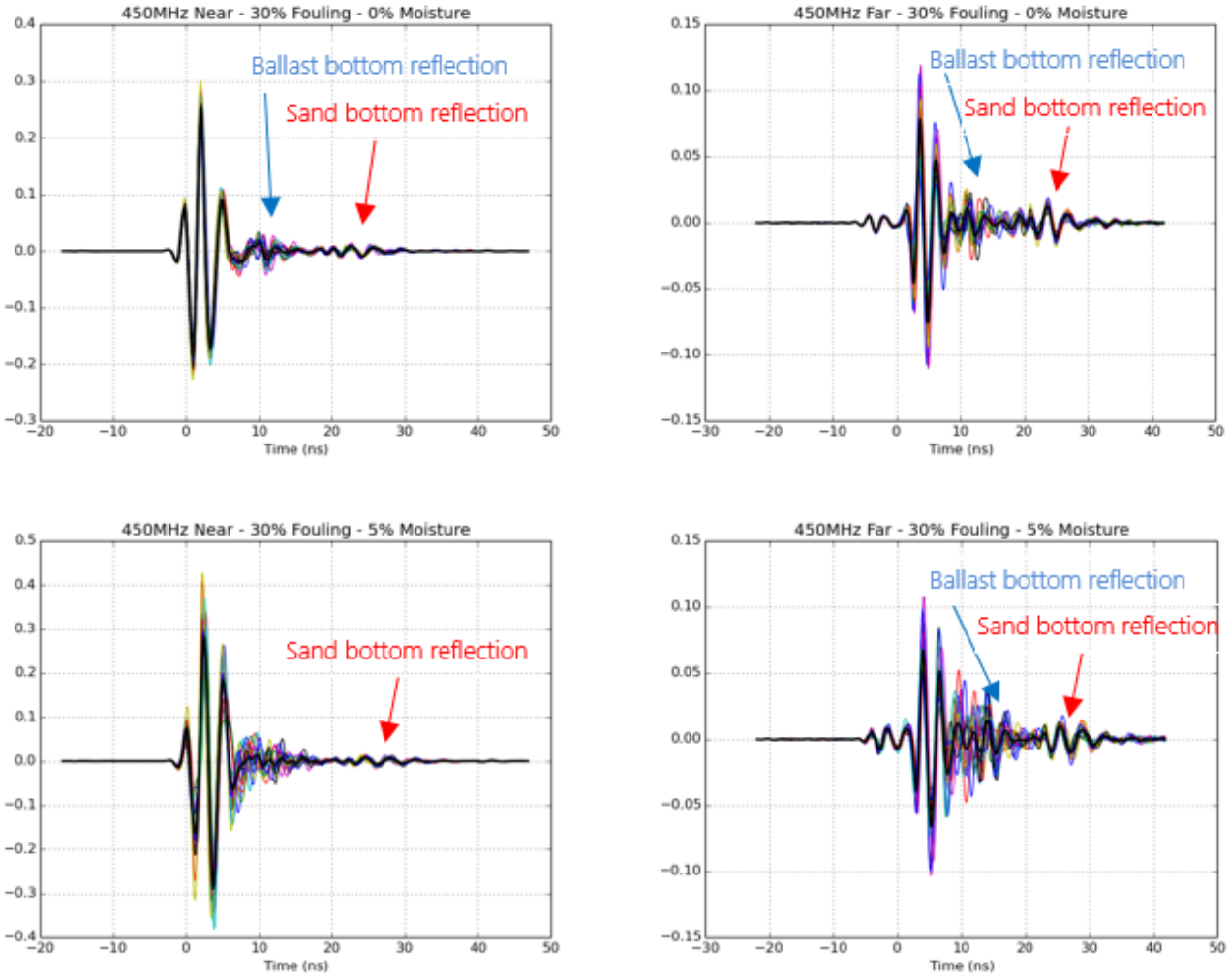

Figure 18. 450 MHz GPR Traces for the 30 Percent Fouled Ballast Model: Dry and Field Capacity

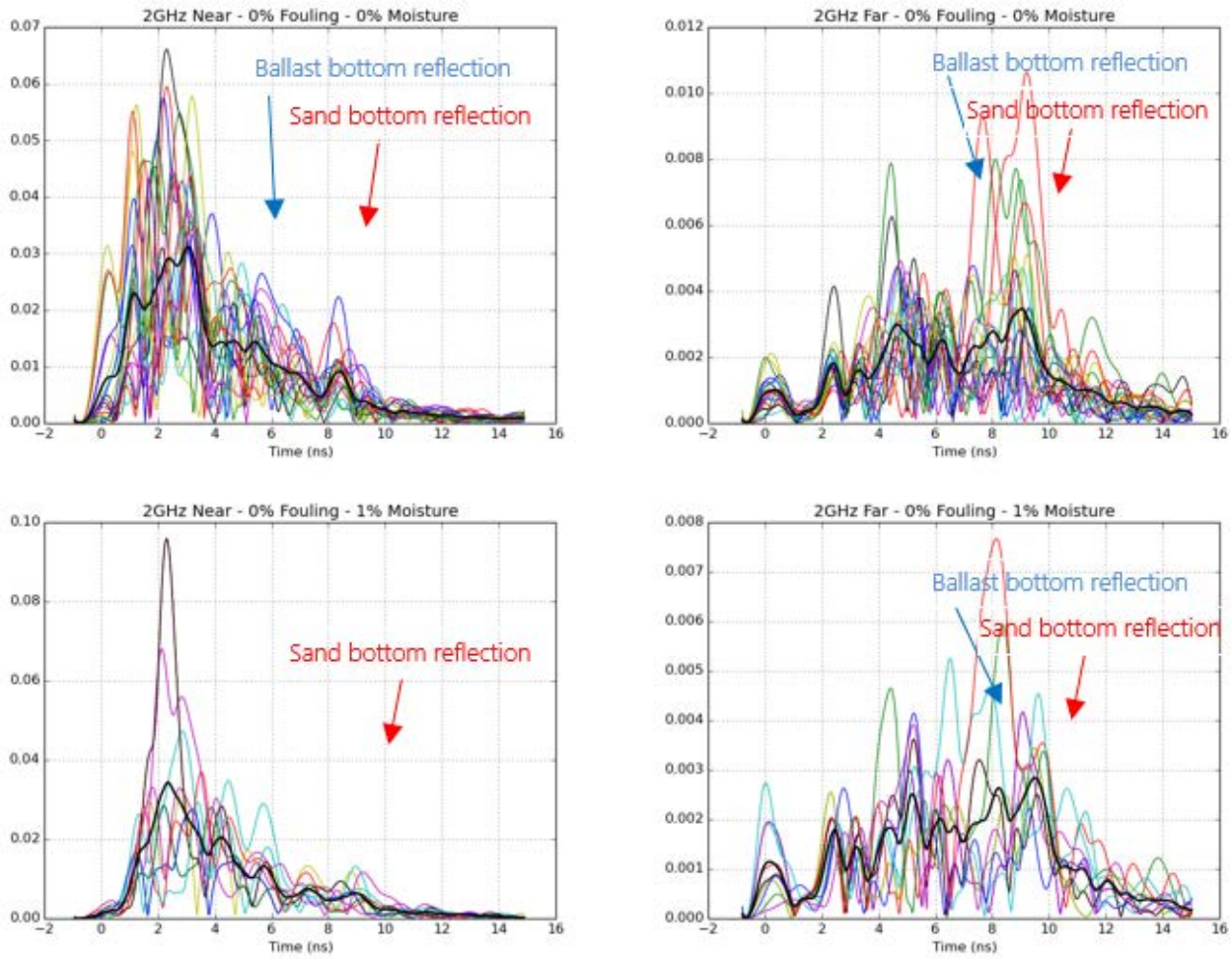

Figure 19. 2 GHz GPR Trace Envelopes for the 0 Percent Fouled Ballast Model: Dry and Field Capacity

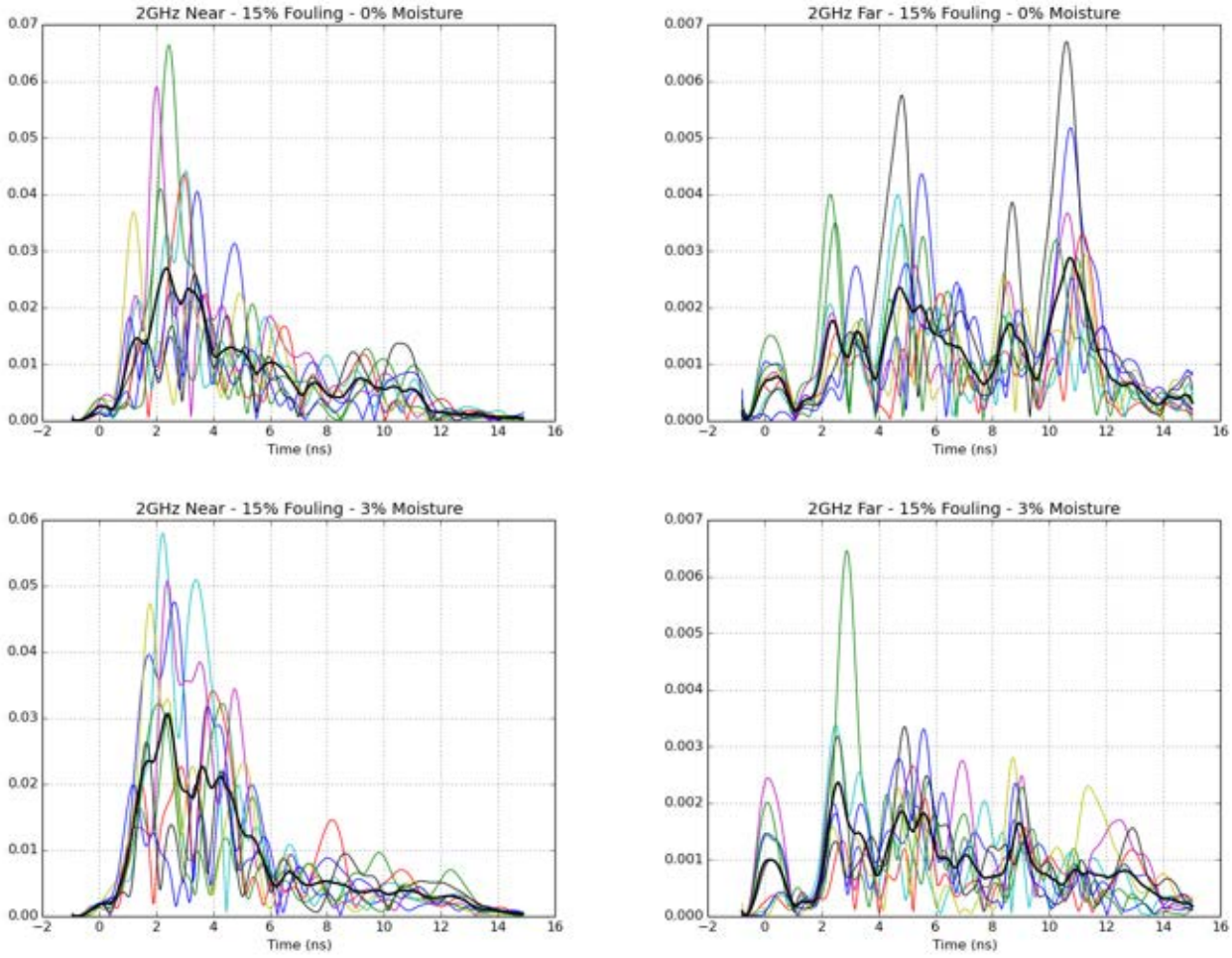

Figure 20. 2 GHz GPR Trace Envelopes for the 15 Percent Fouled Ballast Model: Dry and Field Capacity

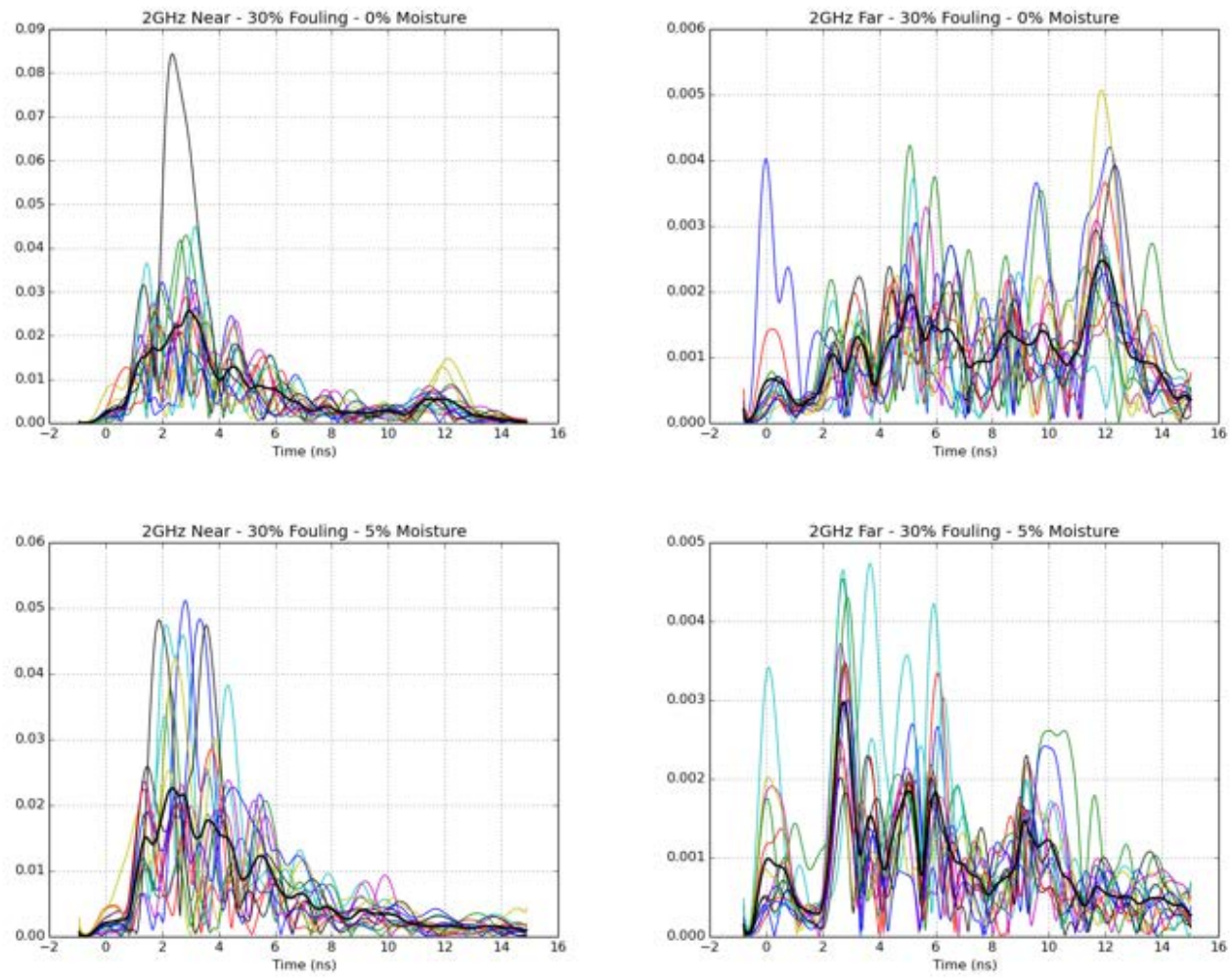

Figure 21. 2 GHz GPR Trace Envelopes for the 30 Percent Fouled Ballast Model: Dry and Field Capacity

5.1.2 Estimating Fouling and Moisture by Multiple Attribute Fitting

As discussed in Section 4.1.2, it is difficult to use the reflected waves to estimate fouling and moisture. Clutter and geologic noise (i.e., localized subsurface inhomogeneity) result in variations in reflected waveforms that make it difficult to pick the arrival time of reflections, and causing a variation in the arrival times that can be identified (see data plots in previous section). Nevertheless, the specular reflection inversion routine was applied to GPR data from the 15 percent fouled ballast model with no moisture because it had high quality reflectors. The routine estimated ballast thickness at 53 cm with a velocity of 0.40 (relative to the EM velocity of free space). The as-built thickness is 60 cm, and the velocity should be around 0.5 for dry ballast.

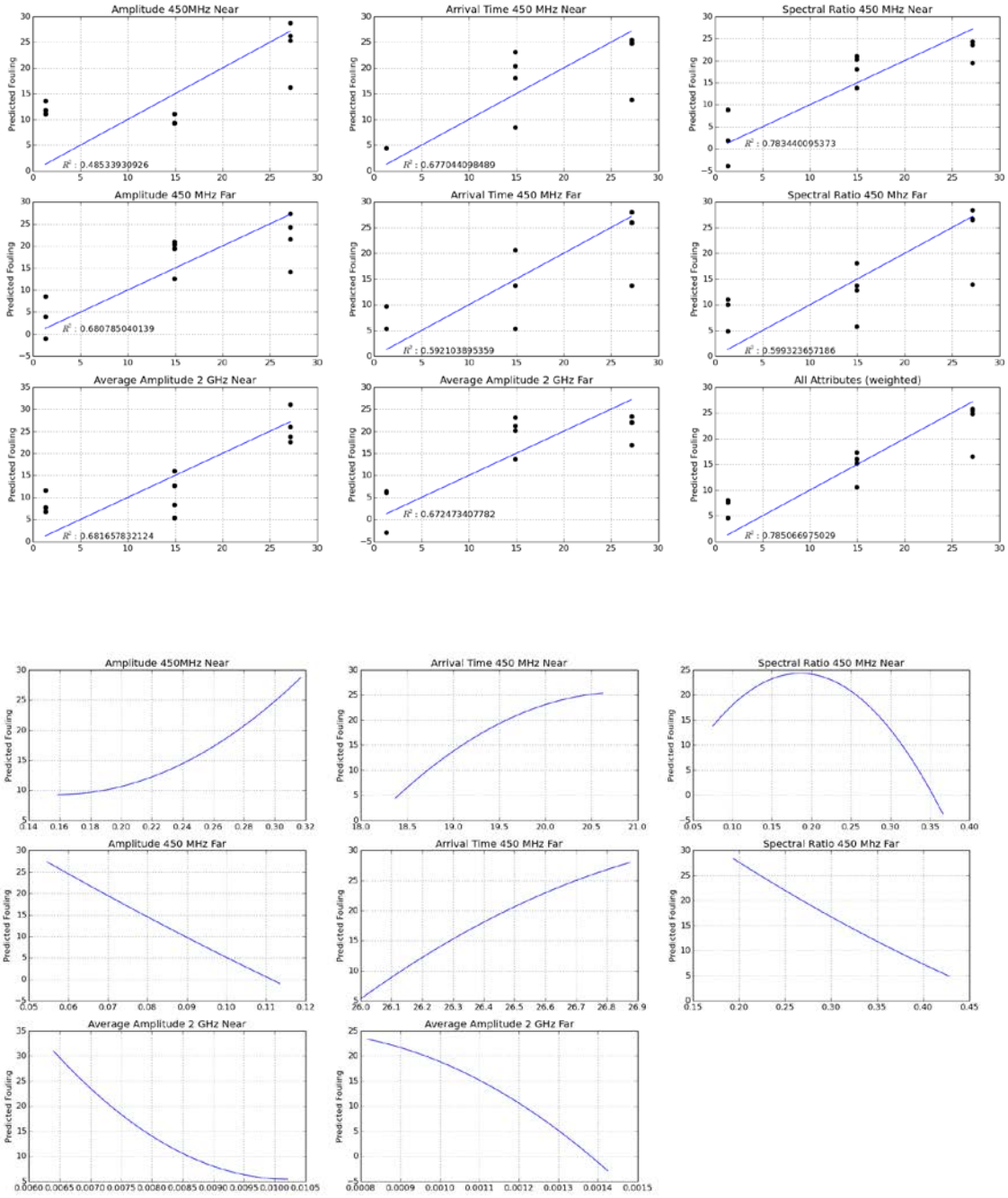

Figure 22. Mapping Relationships Between Direct Waveform Attributes and Fouling

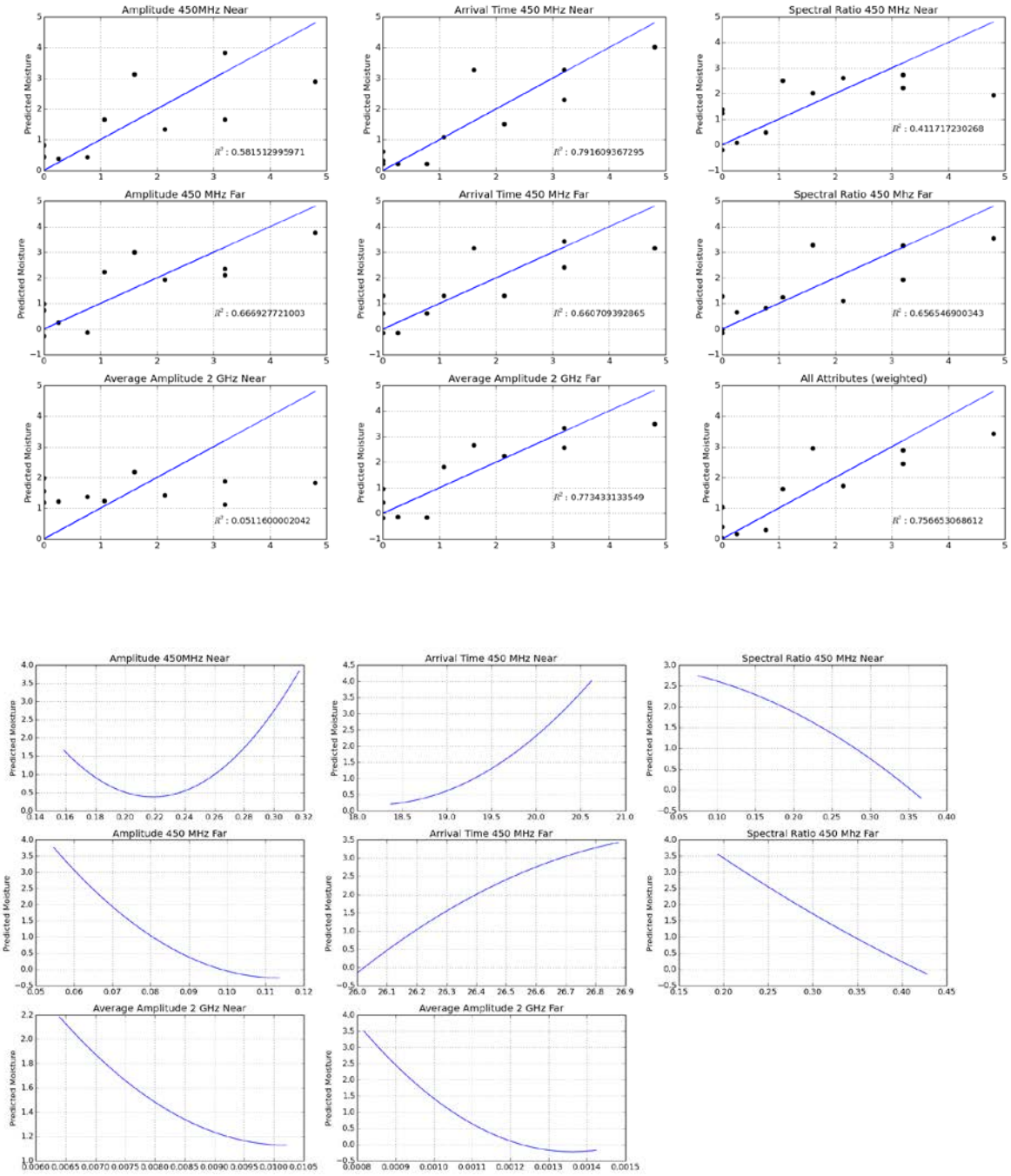

Figure 23. Mapping Relationships Between Direct Waveform Attributes and Moisture

More accurate results require sub-microsecond precision from the survey data. To achieve this, a collection of traces needs to be acquired from different locations in the same vicinity that are stacked to attenuate geologic noise. Additionally, accurate zero-time calibration of the equipment is necessary. The quality of most of the reflected data from other ballast model conditions was too poor to apply the specular reflection inversion routine.

Using the direct wave attributes described in Section 4.1.3, the best fit maps to fouling and moisture were created and shown in Figure 22 and Figure 23. Better R^2 goodness-of-fit values were determined when all the waveforms for each ballast model condition (fouling-moisture) were averaged before extracting the attributes than extracting the attributes from each location and then averaging. From the mixing law and wave propagation physics described in Section 2, we expect monotonic relationships between fouling and moisture, and the extracted attributes. The attributes that do not have monotonic relationships are likely due to poor or insufficient training data and are not used in the combined attribute map. The direct wave amplitudes and spectral ratios appear to have better sensitivity and robustness than the other attributes. The uncertainties in the fouling and moisture values determined by the combined attribute maps are ±4.7% and ±0.75% by weight respectively. Furthermore, since the sensitivity to fine grained material is low unless accompanied by moisture, the ability to estimate fouling should also be critically examined.

5.1.3 GPR Data from the UP Track at Rocky Siding

Physical samples and RABIT GPR data were collected at four different locations on the UP line at Rocky Siding, west of Highway 93, near Arvada, CO. Figure 24 shows a plan view of the location, and all work was completed on the southernmost track (house track). The next track to the north was a siding, and then the main line. Access to siding and mainline tracks is generally only possible when maintenance operations are already scheduled. We spent two partial days in the field and accomplished the GPR surveys quickly, but the physical sampling was more time consuming. We could have surveyed more than four locations and taken more samples, but there was not much variability along the house track and our original plans called for shipping only one pallet of material to the UMass for geotechnical testing.

Figure 24. Aerial View of Rocky Siding in Arvada, CO, Where Field Data was Collected

At each location, physical samples were taken, and at least 150 lbs. of material were sampled (three 5 gallon buckets) in order to have enough material for ASTM GSD tests. Two samples were taken from each location. The first excavation sampled down to the bottom of the tie, and the second excavation sampled the material below the tie. After removing each sample and placing into 5-gallon buckets, the volume of the void in the ground was measured by lining the void with plastic and filling with water up to the top of the tie. The water volume needed to fill the hole represents the sample volume. To measure the volume of the second excavation, the volume of the lined hole was measured and the volume of the first excavation was subtracted. The photos in Figure 25 illustrate the sampling and volume measuring process as well as the

ballast condition. Note that the material being extracted in the lower-right photo is mostly fine-grained. Specific notes for each location are listed below:

- Location 1: Very highly fouled ballast material. The material below the tie appeared to be mostly clay. GPR data were taken at three adjacent cribs numbered from east to west as C3, C1, and C2. Physical samples were taken from the center of the crib C1.
- Location 2: Similar to Location 1, but the material was cleaner at the surface. GPR data were taken at three adjacent cribs numbered from east to west as C1, C2, and C3. Physical samples were taken from the center of the crib C2.
- Location 3: Very highly fouled ballast material. The material below the tie appeared to be mostly clay. GPR data were taken at three adjacent cribs numbered from east to west as C1, C2, and C3. Physical samples were taken from the center of the crib C2.
- Location 4: Only two adjacent cribs were surveyed with the RABIT and sampled at this location. The previous locations appeared to be quite fouled. In order to test the system on cleaner ballast, one crib and the space under the crib were excavated and replaced with nearly fresh ballast obtained from the surface. First, a GPR dataset was collected with the original material in place which was highly fouled ballast material. Then the material in the cribs was excavated and replaced down to the bottom of the ties with fresh ballast, and another GPR dataset was collected. Then the material in both cribs was removed to a depth of 11.5 inches under the tie, as well as the material under the tie. After filling with fresh ballast another GPR survey was made. Then physical samples were collected from the first crib: the first down to the bottom of the tie, and the second to 11.5 inches below the tie.

The physical samples were weighed and sealed into 5-gallon buckets for shipping. A pallet full of buckets was shipped to UMass for testing to determine moisture content and GSD using the same ASTM standards that were employed in the ballast model tests. The results of these tests are listed in Table 5. As multiple samples were not tested at each location, statistical variance is not meaningful. However, the densities listed probably have significant error since in some cases they are different than the expected values. The volume measuring method for rough surfaces as described by Chen et al. (1978) was not used. This would require a collar to be placed over the dig site that matches the hole-size that will be created by the back-hoe, which may be impractical.

Table 5 also lists the estimated moisture and fouling levels (by weight) as determined by the GPR waveform attribute fitting algorithm described above, and these results are plotted in Figure 26. The only attribute used to make these estimates was the direct wave amplitude from the 450 MHz far offset channel. Some of the other attributes had the proper monotonic relationship but were not scaled properly, and others were poorly correlated. This test site probably represents conditions beyond the optimal application of the current version of the RABIT.

Figure 25. Ballast Sampling and Volume Measurement at Rocky Siding in CO with the Ballast Condition (Top), Excavator (Middle), and Volume Measurements (Bottom)

Table 5. Measured and Estimate Properties from UP's Rocky Siding Track Site

Sample Location	Description	Density (g/cc)	Fouling	Estimated Fouling	Moisture	Estimated Moisture
1-above bottom of tie	Visibly appeared extremely fouled	2.2	26.39%	24.98%	8.26%	3.18%
1-below tie	Appeared to be very clay rich	2.14	36.60%		12.23%	
2-above bottom of tie	Visibly appeared fouled	1.75	19.65%	43.27%	7.12%	8.12%
2-below tie	Appeared to be very clay rich	1.95	31.08%		9.58%	
3-above bottom of tie	Visibly appeared extremely fouled	1.62	26.4%	39.48%	4.83%	7.47%
3-below tie	Appeared to be very clay rich	1.86	47.34%		15.81%	
4-from surface to below tie	Clean ballast from surface	1.83	1.75%	3.43%	0.48%	-0.15%

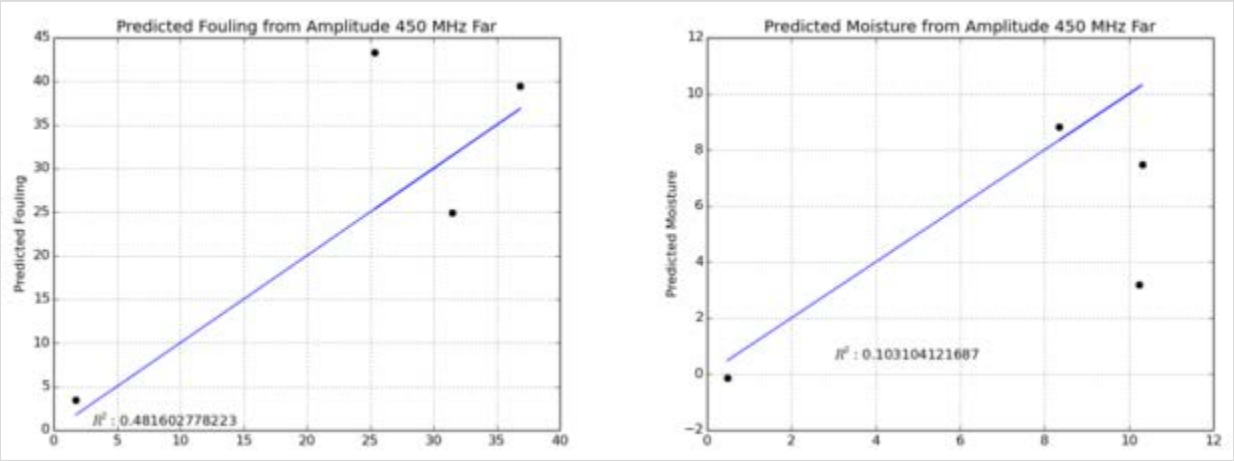

Figure 26. Predicted Fouling and Moisture (By Weight) from GPR Data at the UP Field Site

Figure 27 through Figure 30 shows the GPR data from the UP site. Examination of these figures with the wave attributes in mind that were discussed in Section 4.1.3 leads to the following conclusions.

1. From the sample descriptions and geotechnical test results listed in Table 5, it was expected that the GPR data would indicate very fouled and moist conditions for the first three locations. These fouling and moisture conditions are beyond the range of the ballast model conditions that were built and tested. The ballast conditions at the UP site fall outside the bounds of the data used to create maps between waveform attributes and fouling and moisture levels.
2. The depth of investigation of the direct waves is about a wavelength, which is 30–40 cm for a 450 MHz GPR survey in typical ballast conditions. The direct waves do sense below the ties, but not to a great extent. It is currently unknown how much the condition of the ties affects the measurement when spanning more than one crib. Furthermore, the

effects of shallow variability in EM properties within the direct wave depth of investigation are unknown. Field observations indicate that there was variability within this investigation depth.

3. The arrival time of the 450 MHz near direct wave increases with increasing fouling and moisture as expected, but the same is not true for the 450 MHz far direct wave. Furthermore, the arrival times appear to be shifted from the values obtained from the ballast models. This is likely because the RABIT needed to be calibrated for use in the cold temperatures at the field site (it was just above freezing).
4. The amplitude of the 450 MHz far direct wave increases with decreasing fouling and moisture as expected, but the same is not true for the near waveform. In fact, the near waveform did not have a monotonic relationship even with the training data from the ballast models.
5. The amplitude 2 GHz waveform envelopes did not in general decrease with increasing fouling. It does appear that the decrease does occur at late times (greater than about 4 ns).
6. Location 3 has a clear subsurface reflector visible in the 450 MHz data.

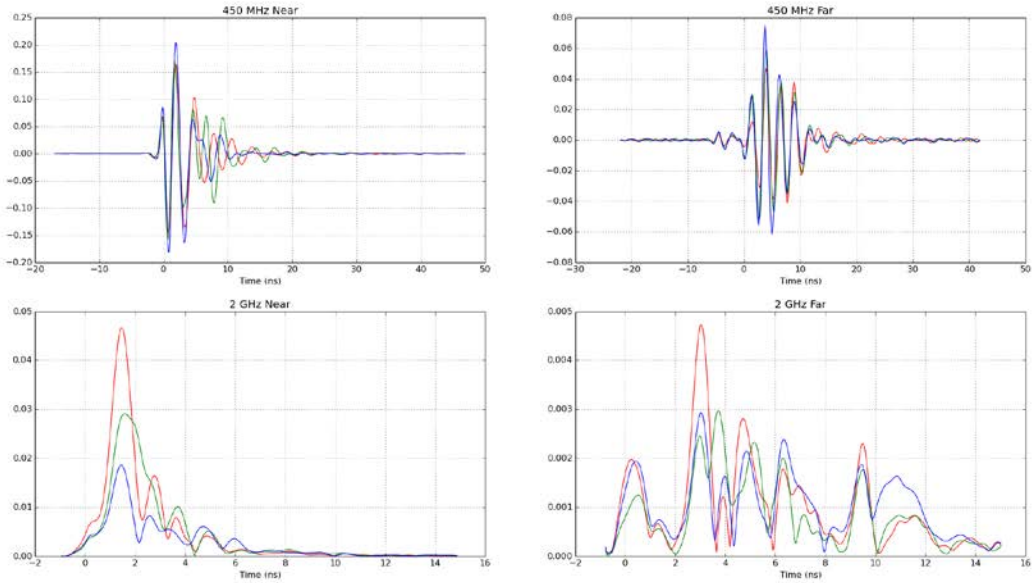

Figure 27. GPR Data from Location 1 on the UP Site

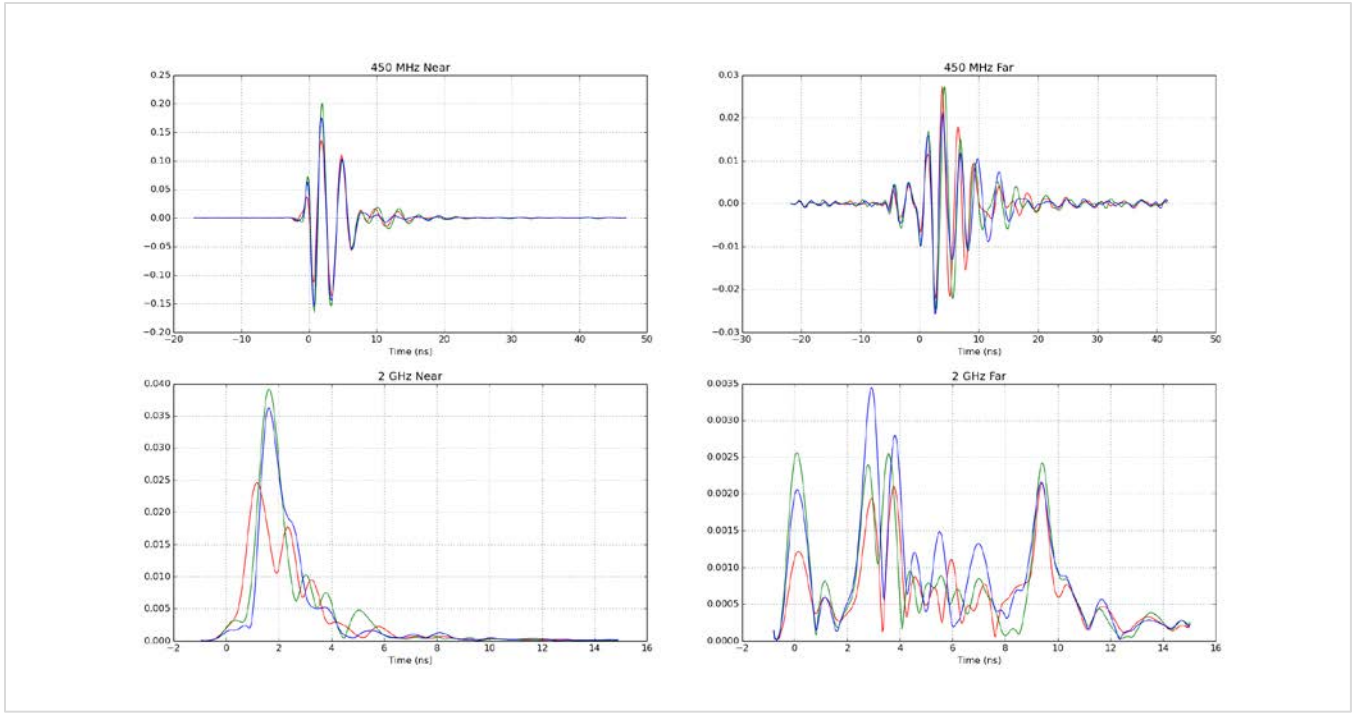

Figure 28. GPR Data from Location 2 on the UP Site

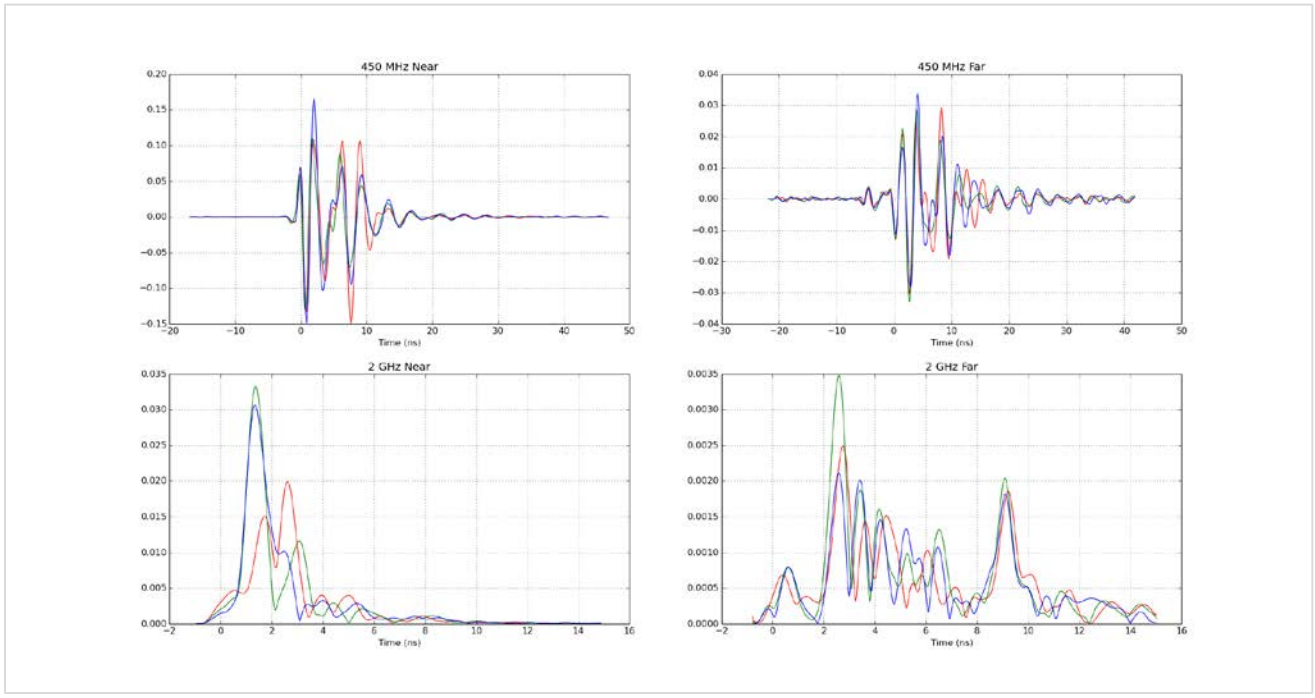

Figure 29. GPR Data from Location 3 on the UP Site

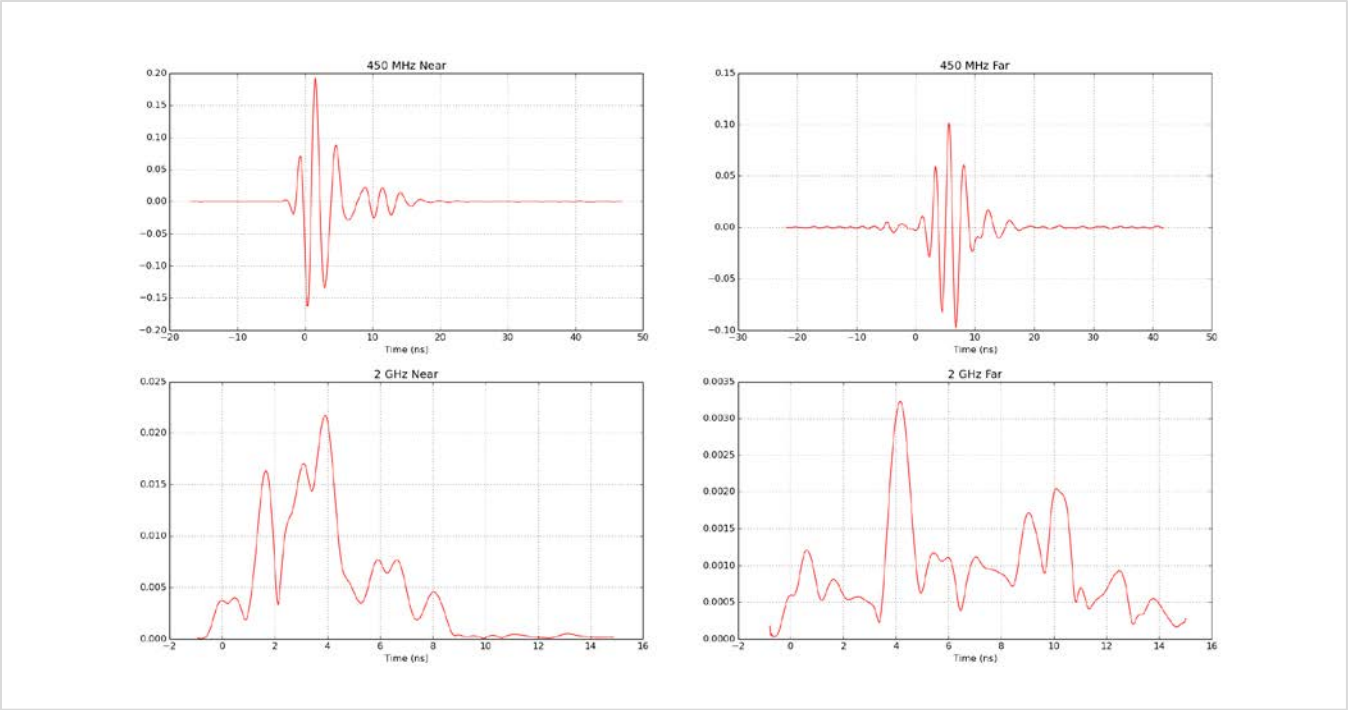

Figure 30. GPR Data from Location 4 on the UP Site

6. Conclusion

Earth Science Systems, LLC (ESS) designed, built, tested, and evaluated data from a prototype GPR ballast inspection system called the RAdar Ballast Inspection Tool (RABIT). The RABIT system could non-invasively estimate the amount of fouling and moisture present in both full-scale ballast models, and in-service track. Results show that fouling and moisture content can be estimated with an uncertainty of about ±4.7% and ±0.75% (by weight) respectively under controlled indoor conditions. Further field testing is needed to develop and evaluate the effectiveness of the analysis methods found in this study.

There are several observations that can be made with the RABIT system. The results show that there is too much variability in the data to analyze reflected waveforms when collecting data from only one or a few locations. While this system is not as unwieldy as the original prototype, it still needs to be made more portable. Also, recording 2 GHz data at two offsets data does not provide significantly more information than a single offset measurement.

After considering these observations, it is recommended that the RABIT system evolve into two different versions. The first is a small very lightweight single-offset 2 GHz model that measures back scattering. This version would measure approximately 9 × 9 × 6 inches (23 × 23 × 15 cm) and weigh about 8 lbs. (3.6 kg). It could be used to scan one or many locations to get a representative assessment. With its small size and footprint, it could scan cribs and shoulders, and could be used close to the rail. The second system would be similar to the existing system, and use ESS' new thin antenna technology to make dual-offset 450 MHz measurements and a single-offset 2 GHz measurement. It would span two cribs (rather than three for the current instrument), and weigh about 30 lbs. (14 kg). It would also have wheels that run across the crib or along the rails so that continuous data along a few or many cribs can be collected. This would enable reflected wave analysis. Surveys conducted from a fixed height from equipment resting on the rails may provide more uniform antenna coupling. ESS is currently developing an embedded computer so that future versions of the RABIT will not require an external data acquisition computer as seen in Figure 3.

From both theoretical analysis and experimental results, the sensitivity of GPR scans to moisture content is evident. This work agrees with the findings of previous researchers in demonstrating that increased fouling and moisture attenuate high-frequency components of GPR waveforms (Al-Qadi et al., 2007) (Levomakit et al., 2010). However, the measurement is primarily sensitive to changes in moisture, with less sensitivity to changes in fouling. It is quite likely that the response to fouling seen by previous researchers is primarily due to moisture. A certain level of moisture implies a certain level of fouling (need fine grained material to hold moisture), but the presence of fouling does not imply moisture. In effect, a given moisture level implies at least a corresponding amount of fine-grained material, and there could be more fine-grained material that could hold more moisture if it were present. This raises the following question: What is the relationship between fouling, moisture, and ballast resiliency and load capacity? Intuitively, moisture will degrade ballast performance more than the presence of dry fine-grained material. An investigation of the relationships between fouling, moisture, and strength properties of ballast has been planned for the next phase of this project.

Advanced full-waveform forward modeling and inversion algorithms have been created, with the main purpose of analyzing reflected waveforms. These routines account for both specular (layer-cake) wave propagation and for random volume scattering. Unfortunately, the ground-coupled

GPR data from the ballast models contain a large response to the geologic noise and clutter (i.e., spatial variability in fouling, moisture, and other subsurface properties). In many cases, this unwanted response cannot be distinguished from the actual reflections with only data from a single location. As a result, these algorithms have only received minimal testing. During this study, it was proven that full-waveform analysis does provide information about fouling and moisture and may be able to provide otherwise unknown information, such as porosity and nominal void diameter.

These routines simply need continuous data along the track to be able to separate reflections from geologic noise and clutter. More uniform antenna coupling from a fixed height will also help. Continuous data can also provide information about non-continuous features such as ballast pockets and clay lenses. These possibilities, together with the fact that these routines can also be applied to continuous GPR data collected from moving vehicles, warrants further testing of these full-waveform routines. It may be possible to add direct wave processing to the routines as well.

A multi-attribute fitting routine was created that extracts waveform attributes from direct wavelets and waveform envelopes, and maps these attributes to fouling and moisture. This approach proved successful, largely because the selected attributes can easily be extracted from noisy waveforms. Data measured from the ballast models were used to obtain the mapping functions, and the variations in this data resulted in uncertainties in the mapping functions (±4.7% fouling and ±0.75% moisture by weight). Our preliminary assessment is that the direct wave amplitudes and spectral ratios will be the most sensitive and robust attributes. If a dataset for determining the mapping relationships can be obtained with less variation in the GPR waveforms by continuously recording data, the calibration uncertainties can be reduced. More testing in field conditions would be needed to thoroughly vet these algorithms.

A method for building ballast models was created that provides a high-quality specimen for conducting GPR and geotechnical tests. There was 5–10 percent uncertainty in the density and void ratios of samples taken from these models (see Table 3). There was likely more variation in the distribution of fine-grained material and moisture. As seen in smaller representative specimens, irrigation flushes the fine-grained material downwards. It took a significant but reasonable amount of effort to build these models, and the degree of uniformity obtained is as high as reasonably achievable.

The prototype equipment and algorithms created for this project have shown promise in being able to non-destructively assess moisture. To date however, very little field work has been completed. More field testing is needed so that the equipment and algorithms can be improved, and the applicability demonstrated. The processing routines need to be able to operate in the field so that the operator can be assured that good data are being collected and good results are being obtained. Finally, in an effort to streamline field testing, we recommend collecting smaller samples for ground truth than the 70-kg specified by ASTM standards so that more samples can be transported and analyzed with the available resources. A significant field work component has been planned for the next phase of this project.

7. References

Al-Qadi, I., Wie, X., and Roberts, R. (2007, January). "Scattering analysis of railroad ballast using ground penetrating radar." Transportation Research Board Annual Meeting. *NDT & E International*, *41*(6): Washington, DC.

AREMA. (2010). Manual for Railway Engineering, American Railway Engineering & Maintenance-of-Way Association.

ASTM. (2007). Annual Book of Standards, Volume 04.08, Soil and Rock (1): D420–D4914, ASTM: Philadelphia, PA.

ASTM. (2008). Annual Book of Standards, Volume 04.08, Soil and Rock (II): D5714–Latest, ASTM: Philadelphia, PA.

Chen, H. M., and Yoo, T. S. (1978, March). Railroad Ballast Density Measurement, *Geotechnical Testing Journal*, *1*(1), pp. 41–54.

Hufford, G. A., Liebe, H. J., and Manabe, T. (1991). A model for the complex permittivity of water at frequencies below 1 THz. *Journal of Infrared, Millimeter, and Terahertz Waves*, *12*(7).

Kong, J.A., and Tsang, L. (2001). Scattering of Electromagnetic Waves, Wiley and Sons: New York, pp. 413.

Levomaki, M., Nurmikolu, A., Silvast, M., and Wiljanen, B. (2010). An Inspection of Railway Ballast Quality Using Ground Penetrating Radar in Finland, Proceedings of the Institution of Mechanical Engineers, Part F: Journal of Rail and Rapid Transit, *224*(345).

Selig, E. T., and Waters J. M. (1994). Track Geotechnology and Substructure Management. T. Telford, London.

Sihvola, A. H. (1999). Electromagnetic Mixing Formulas and Applications. IEE Publishing, London.

Abbreviations and Acronyms

ESS	Earth Science Systems, LLC
EM	Electromagnetic
FCC	Federal Communication Commission
FRA	Federal Railroad Administration
GSD	Grain-Size Distribution
GPR	Ground Penetrating Radar
RABIT	RAdar Ballast Inspection Tool
UP	Union Pacific Railroad
UMass	University of Massachusetts